J|A|C|S
ARTICLES
Published on Web 07/04/2006

d-Orbital Effects on Stereochemical Non-Rigidity: Twisted Ti^{IV} Intramolecular Dynamics

Anna V. Davis,[†] Timothy K. Firman,[‡] Benjamin P. Hay,[‡] and Kenneth N. Raymond*[,†]

Contribution from the Department of Chemistry, University of California, Berkeley, California 94720-1460, and Chemical Sciences Division, Pacific Northwest National Laboratory, P.O. Box 999, Richland, Washington 99352

Received March 15, 2006; E-mail: raymond@socrates.berkeley.edu

Abstract: The isomerization dynamics of tris-catecholate complexes have been investigated by variable-temperature NMR methods, demonstrating that the intramolecular racemization of Δ and Λ enantiomers of d^0 Ti^{IV} is facile and faster than that of d^{10} Ga^{III} and Ge^{IV} analogues. Activation parameters for the racemization of K_2[Ti**2**$_3$] (H_2**2** = 2,3-dihydroxy-*N,N′*-diisopropylterephthalamide) were determined from line shape analysis of ^{1}H NMR spectra {methanol-d_4: $\Delta H^{\ddagger} = 47(1)$ kJ/mol; $\Delta S^{\ddagger} = -34(4)$ J/molK; $\Delta G^{\ddagger}_{298} = 57(3)$ kJ/mol; DMF-d_7: $\Delta H^{\ddagger} = 55(1)$ kJ/mol; $\Delta S^{\ddagger} = -16(4)$ J/molK; $\Delta G^{\ddagger}_{298} = 59(3)$ kJ/mol; D_2O (pD* = 8.6, 20% MeOD): $\Delta H^{\ddagger} = 48(3)$ kJ/mol; $\Delta S^{\ddagger} = -28(10)$ J/molK; $\Delta G^{\ddagger}_{298} = 56(3)$ kJ/mol}. The study of K_2[Ti**4**$_3$] (H_2**4** = 2,3-dihydroxy-*N*-*tert*-butyl-*N′*-benzylterephthalamide) reveals two distinct isomerization processes: faster racemization of *mer*-[Ti**4**$_3$]$^{2-}$ by way of a Bailar twist mechanism (D_{3h} transition state) {$T_c \approx 242$ K, methanol-d_4}, and a slower *mer*⇌*fac* [Ti**4**$_3$]$^{2-}$ isomerization by way of a Rây−Dutt mechanism (C_{2v} transition state) {$T_c \approx 281$ K, methanol-d_4}. The solution behavior of the Ti^{IV} complexes mirrors that reported previously for analogous Ga^{III} complexes, while that of analogous Ge^{IV} complexes was too inert to be detected by ^{1}H NMR up to 400 K. These experimental findings are augmented by DFT calculations of the ML_3 ground states and Bailar and Rây−Dutt transition states, which correctly predict the relative kinetic barriers of complexes of the three metal ions, in addition to faithfully reproducing the ground-state structures. Orbital calculations support the conclusion that participation of the Ti^{IV} d orbitals in ligand bonding contributes to the greater stabilization of the prismatic Ti^{IV} transition states.

Introduction

The stereochemical nonrigidity of six-coordinate metal−ligand complexes is a classic topic in modern coordination chemistry, recognized by Alfred Werner,[1,2] and with important bearing on areas such as catalysis,[3] bioinorganic chemistry,[4,5] and materials chemistry.[6] Six-coordinate complexes of two or three bidentate chelates can exist as stereoisomers (Δ and Λ) as well as geometrical isomers (*fac* and *mer*, which are also referred to as *cis* and *trans*), and the interconversion of these isomers may occur over a large range of time scales and by a number of different mechanisms.[7,8] In a particularly dramatic example, a Co^{III} tris-tropolonate was found to racemize at a rate 10^{11} times faster than that of a Co^{III} tris-β-diketonate, a result partially explained by a difference in mechanism.[9,10] While rigorous study of several series of tris-chelate metal complexes (ML_3) has led to the development of general relationships between the properties of a complex and its mechanism and relative rate of isomerization, there are notable outliers. Here such an unanticipated trend in ML_3 isomerization rates is identified and resolved with the application of current metal−ligand bonding concepts to transition-state structure and supporting density functional theory calculations.

Intramolecular isomerization mechanisms of ML_3 complexes are classified with respect to the changes in metal coordination they involve. Fully dissociative mechanisms involving the loss

[†] University of California.
[‡] Pacific Northwest National Laboratory.

(1) Werner, A. *Ann.* **1912**, *386*, 1−272.
(2) Werner, A. *Ber.* **1911**, *44*, 3279−3284; Werner, A. *Ber.* **1911**, *44*, 2445−2455.
(3) Brunner, H. *Angew. Chem., Int. Ed.* **1999**, *38*, 1194−1208; Brunner, H. *Eur. J. Inorg. Chem.* **2001**, 905−912; Ganter, C. *Chem. Soc. Rev.* **2003**, *32*, 130−138; Faller, J. W. *New J. Chem.* **2003**, *27*, 899−901; Knight, P. D.; Scott, P. *Coord. Chem. Rev.* **2003**, *242*, 125−143; Walsh, P. J.; Lurain, A. E.; Balsells, J. *Chem. Rev.* **2003**, *103*, 3297−3344.
(4) Dertz, E. A.; Raymond, K. N. In *Comprehensive Coordination Chemistry II*; McCleverty, J., Meyer, T., Eds.; Pergamon: Oxford, 2003; Vol. 8, pp 141−168; Matzanke, B. F.; Müller-Matzanke, G.; Raymond, K. N. In *Physical Bioinorganic Chemistry Series*; Loehr, T. M., Ed.; VCH Publishers: New York, 1989; pp 1−121; Erkkila, K. E.; Odom, D. T. *Chem. Rev.* **1999**, *99*, 2777−2795; Metcalfe, C.; Thomas, J. A. *Chem. Soc. Rev.* **2003**, *32*, 215−224; Lieberman, M.; Tabet, M.; Sasaki, T. *J. Am. Chem. Soc.* **1994**, *116*, 5035−5044; Schneider, J. P.; Kelly, J. W. *Chem. Rev.* **1995**, *95*, 2169−2187; Bernauer, K.; Ghizdavu, S.; Verardo, L. *Coord. Chem. Rev.* **1999**, *190−192*, 357−369.
(5) Kersting, B.; Telford, J. R.; Meyer, M.; Raymond, K. N. *J. Am. Chem. Soc.* **1996**, *118*, 5712−5721.
(6) James, S. L. *Chem. Soc. Rev.* **2003**, *32*, 276−288; Kesanli, B.; Lin, W. *Coord. Chem. Rev.* **2003**, *246*, 305−326; Han, L.; Hong, M. *Inorg. Chem. Commun.* **2005**, *8*, 406−419; Rosseinsky, M. J. *Microporous Mesoporous Mater.* **2004**, *73*, 15−30.
(7) Basolo, F.; Pearson, R. G. *Mechanisms of Inorganic Reactions*, 2nd ed.; John Wiley and Sons: New York, 1967.
(8) Serpone, N.; Bickley, D. G. *Prog. Inorg. Chem.* **1972**, *17*, 391−566.
(9) Eaton, S. S.; Hutchison, J. R.; Holm, R. H.; Muetterties, E. L. *J. Am. Chem. Soc.* **1972**, *94*, 6411−6425.
(10) Eaton, S. S.; Eaton, G. R.; Holm, R. H.; Muetterties, E. L. *J. Am. Chem. Soc.* **1973**, *95*, 1116−1124.

10.1021/ja0617946 CCC: $33.50

of one ligand to form a four-coordinate intermediate species (ML_2) have been described but are rare,[11,12] with intramolecular mechanisms cited in the majority of ML_3 studies.[7,8] Bond-rupture isomerizations proceed via a five-coordinate species formed by the dechelation of one bidentate ligand (i.e. one of two M−L bonds is broken).[1,7,13] Nonbond-rupture mechanisms retain the six-coordinate nature of the complex throughout the isomerization process and may be further characterized by the symmetry of their respective transition states. For an octahedral complex, rotation of the ligands around any of the four C_3 axes leads to a trigonal prismatic transition state. For a tris-bidentate complex the symmetry is reduced, so that only one of these C_3 axes remains. The trigonal or Bailar twist is defined by a D_{3h} transition state generated as the three ML_3 chelates pivot around the C_3 axis of the D_3-symmetric complex.[14,15] In the rhombic or Rây−Dutt twist, the chelating ligands rotate around a pseudo-C_3 axis of the complex (a C_3 axis of the octahedron defined by complex's donor atoms which is not a C_3 axis of the D_3 ML_3 complex) to generate a C_{2v} symmetric transition state.[16,17]

Experimental differentiation between the Rây−Dutt and Bailar pathways can be difficult. However, for unsymmetrical chelates, the mechanisms can be distinguished on the basis of the interconversion of geometric isomers. Tris complexes of unsymmetrical chelates, $M(aa')_3$, can exist as either facial (*fac*) or meridional (*mer*) isomers, or as a mixture of both. As demonstrated in Figure 1, the rhombic twist interconverts *fac* and *mer* isomers, whereas the trigonal twist does not. For complexes which racemize relatively rapidly, measurement of *mer*⇌*fac* isomerization may be especially difficult. Fay and Piper[15] and Holm and co-workers[18] pioneered NMR line shape analysis in the study of tris-chelate isomerization. The use of diastereotopic groups and unsymmetrical chelates facilitates the separation of racemization and geometrical isomerization events.

Like the Rây−Dutt twist, the bond-rupture mechanism allows for the interconversion of stereoisomers. A trigonal-bipyramidal intermediate with a dangling ligand in the axial position causes geometrical isomerization with inversion of stereochemistry, while the intermediate with a dangling ligand in the equatorial position produces geometrical isomerization without inversion of stereochemistry.[12] Experimentally, bond rupture is indicated by high $\Delta H^{\ddagger}$ and positive $\Delta S^{\ddagger}$ values.[12] Dependence of isomerization rates on solvent, counterions, and pH are also diagnostic of a bond-rupture pathway.[7,12]

Trends correlating mechanism and rate of ML_3 isomerization to chelate type and metal ion have emerged through a number

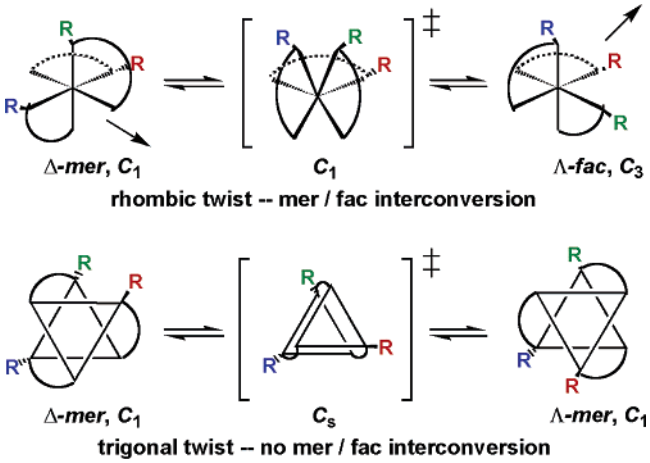

Figure 1. Unsymmetrical chelates are used to differentiate twist mechanisms. The rhombic twist interconverts *mer* and *fac* isomers (top), while the trigonal twist does not (bottom). The three-fold axis of the tris chelate (which is not a true C_3 axis for the *mer* configurations of the unsymmetrical chelate) is indicated with an arrow in the top scheme. This axis is perpendicular to the page in the bottom scheme. Substituents are colored only to aid viewing.

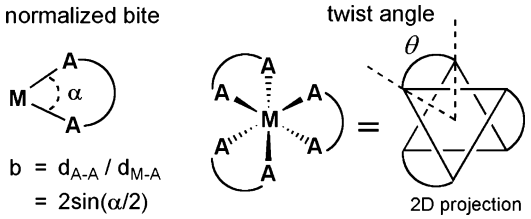

Figure 2. Normalized bite (b) and twist angle (θ) metrics defined by Kepert to describe tris-chelate complexes.[24] The six-coordinate tris-chelate complex is viewed down its C_3 axis (center and right).

of elegant investigations.[9,10,15,18−22] Kepert has parametrized some of these relationships, defining metrics of chelate complexes on the basis of an electrostatic model.[23,24] Complexes with larger normalized bite (b) values, larger chelates, and/or shorter metal−ligand bonds, tend to have larger twist angles (θ) and slower rates of isomerization (Figure 2).[24,25] As Kepert has pointed out, these trends accurately describe relationships among the most well-studied classes of tris-chelates in which electronic considerations, such as ligand field stabilization energy do not play a significant role.[26,27] β-Diketonate ML_3 complexes have larger normalized bite values ($b \approx 1.4$) and slower rates of isomerization than tropolonate complexes ($b \approx 1.3$) which are then slower than the dithiocarbamates ($b \approx 1.2$).

(11) Thomas, W. *J. Chem. Soc.* **1921**, *119*, 1140−1145; Thomas, W.; Fraser, R. *J. Chem. Soc.* **1923**, *123*, 2973−2976; Wilkins, R. G.; Williams, M. J. G. *J. Chem. Soc.* **1957**, 1763−1769; Broomhead, J. A. *Aust. J. Chem.* **1963**, *16*, 186.
(12) Wilkins, R. G. *The Study of Kinetics and Mechanism of Reactions of Transition Metal Complexes*; Allyn and Bacon, Inc.: Boston, 1974.
(13) Werner, A. *Ber.* **1912**, *45*, 3061−3070.
(14) Bailar, J. C., Jr. *J. Inorg. Nucl. Chem.* **1958**, *8*, 165−175; More recently, the Bailar twist has been analyzed as the minimal distortion path between octahedron and trigonal prism by continuous symmetry maps and shape classification: Alvarez, S.; Avnir, D.; Llunell, M.; Pinsky, M. *New J. Chem.* **2002**, *26*, 996−1006; Casanova, D.; Cirera, J.; Llunell, M.; Alemany, P.; Avnir, D.; Alvarez, S. *J. Am. Chem. Soc.* **2004**, *126*, 1755−1763.
(15) Fay, R. C.; Piper, T. S. *Inorg. Chem.* **1964**, *3*, 348−356.
(16) Rây, P.; Dutt, N. K. *J. Indian Chem. Soc.* **1943**, *20*, 81−92.
(17) Brady argues that the Rây−Dutt and Bailar mechanisms are equivalent as both involve twisting around a C_3 axis (pseudo or real), while Springer and Sievers note that the opposite rotational motion in the Rây−Dutt twist produces the Bailar transition state. The two mechanisms are most commonly defined by their respective transition-state symmetries; Brady, J. E. *Inorg. Chem.* **1969**, *8*, 1208−1209; Springer, C. S., Jr.; Sievers, R. E. *Inorg. Chem.* **1967**, *6*, 852−854.
(18) Gordon, J. G., II; Holm, R. H. *J. Am. Chem. Soc.* **1970**, *92*, 5319−5332.
(19) Hutchison, J. R.; Gordon, J. G., II; Holm, R. H. *Inorg. Chem.* **1971**, *10*, 1004−1017.
(20) Pignolet, L. H.; Lewis, R. A.; Holm, R. H. *J. Am. Chem. Soc.* **1971**, *93*, 360−371.
(21) Palazzotto, M. C.; Duffy, D. J.; Edgar, B. L.; Que, L., Jr.; Pignolet, L. H. *J. Am. Chem. Soc.* **1973**, *95*, 4537−4545.
(22) Que, L., Jr.; Pignolet, L. H. *Inorg. Chem.* **1974**, *13*, 351−356; Duffy, D. J.; Pignolet, L. H. *Inorg. Chem.* **1974**, *13*, 2045−2050.
(23) Kepert, D. L. *Inorg. Chem.* **1972**, *11*, 1561−1563; Kepert, D. L. *Inorganic Sterochemistry*; Springer-Verlag: Berlin, 1982; Vol. 6.
(24) Kepert, D. L. *Prog. Inorg. Chem.* **1977**, *23*, 1−65.
(25) The "bite angle" (α) may be more familiar terminology to many readers. As we note, normalized bite is related to bite angle and follows similar trends. Larger bite angles correspond to larger normalized bites. The normalized bite analysis emphasizes the contribution of both metal−ligand bond distance and ligand bite (d_{A-A}) which we find useful in our analysis.
(26) In a notable example, the fluxionality of Os tris-(3,5-di-*tert*-butylquinone) (DBQ), in contrast to the stereochemical rigidity of the Ru analogue, was ascribed to a subtle difference in charge distribution and electronic structure between the two complexes: ref 27.
(27) Bhattacharya, S.; Boone, S. R.; Fox, G. A.; Pierpont, C. G. *J. Am. Chem. Soc.* **1990**, *112*, 1088−1096.

For all three classes of ligands, isomerizaton rates also tend to increase with the ionic radius of the metal: larger metals have longer metal−ligand bond lengths and thus smaller *b* values.

Mechanistically, bond-rupture mechanisms are commonly implicated for the β-diketonate complexes,[15,18,19,28] whereas nonbond-rupture twist mechanisms predominate for the tropolonate and dithiocarbamate complexes.[9,10,20−22] It has been proposed that greater chelate rigidity may favor twist mechanisms and faster rates.[9] Correlations between a complex's ground-state structure (as determined in the solid state) and isomerization rate have also been found, demonstrating that less twisted structures often isomerize faster.[20,21] Kepert-type analysis leads to the same prediction, since lower twist angles are related to smaller *b* values.[24] However the d-electron configuration of a metal ion can override these structural factors, and ligand field stabilization energy calculations have also been demonstrated to be a reliable predictor of isomerization rate.[21,22]

Previous study of gallium (III) tris-catecholate complexes, $[Ga(cat)_3]^{3-}$, supported the predominance of an intramolecular twist mechanisms,[5,29] a result consistent with studies of the similar Ga^{III} tris-tropolonate complexes.[19,30] The slower racemization rate of the catecholate structure would also be predicted on the basis of its slightly larger normalized bite. The isomerization behavior of analogous Ti^{IV} and Ge^{IV} tris-catecholate (cat) complexes are presented here. Both $[Ti(cat)_3]^{2-}$ and $[Ge(cat)_3]^{2-}$ have been reported[31] and structurally characterized.[32,33] The tremendous thermodynamic stability of the $[Ti(cat)_3]^{2-}$ complex is evidenced by a shift of the Ti^{IV}/ Ti^{III} reduction potential (NHE) from 0.099 to −1.14 V.[32] Foreshadowing the present studies, Rosenheim and co-workers reported in 1931 an attempted resolution of $[Ti(cat)_3]^{2-}$ by precipitation with cinconinium (cinc).[34] While the Ti^{IV} complex was optically active as a diastereomeric salt, cation exchange for an achiral counterion resulted in optically inactive material. Rosenheim speculated that fast racemization of $[Ti(cat)_3]^{2-}$ was likely. Now, some 70 years later, this isomerization is revisited with modern spectroscopic techniques. Current understanding of d-orbital interactions, supported by DFT calculations, adds a new dimension to the analysis of stereochemical nonrigidity.

Results and Discussion

Tris-catecholate Ti^{IV} Complexes. Four Ti^{IV}-tris-catecholate complexes were examined in the study of $[Ti(cat)_3]^{2-}$ isomerization, and these complexes were derived from 2,3-dihydroxy-*N*-isopropylbenzamide (H_2**1**), 2,3-dihydroxy-*N*,*N*′-diisopropyl-terephthalamide (H_2**2**), 2,3-dihydroxy-*N*-methylbenzamide (H_2**3**), and 2,3-dihydroxy-*N*-*tert*-butyl-*N*′-benzyl-terephthalamide (H_2**4**) (Figure 3). The $[Ti\mathbf{1}_3]^{2-}$, $[Ti\mathbf{2}_3]^{2-}$ and $[Ti\mathbf{3}_3]^{2-}$ complexes were initially evaluated to probe relative contributions of racemization and geometrical interconversion to the isomerization mechanism of $[Ti(cat)_3]^{2-}$ compounds. The isopropyl methyl groups of ligands H_2**1** and H_2**2** are enantiotopic and therefore become diastereotopic in the chiral Δ- and Λ-$[TiL_3]^{2-}$ complexes. As will be described, the diastereotopic methyl groups serve as a ^{1}H NMR handle for monitoring ML_3 stereoinversion. The C_{2v} symmetric ligand H_2**2** produces only Δ- and Λ-$[TiL_3]^{2-}$ stereoisomers—no geometrical isomers are possible—and therefore $M\mathbf{2}_3$ complexes solely probe ML_3 racemization. Complexes of ligands H_2**1**, H_2**3**, and H_2**4** can exist as *fac* and *mer* isomers: $[Ti\mathbf{1}_3]^{2-}$ reports both racemization and geometrical isomerization, while $[Ti\mathbf{3}_3]^{2-}$ detects only geometrical isomerization.

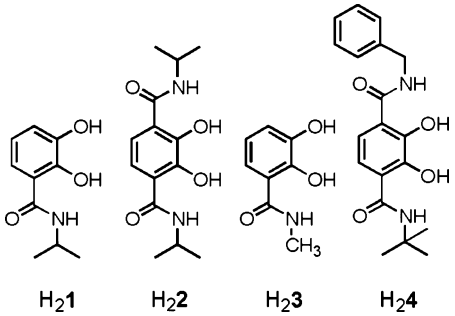

Figure 3. Ligands H_2**1**, H_2**2**, H_2**3**, and H_2**4**.

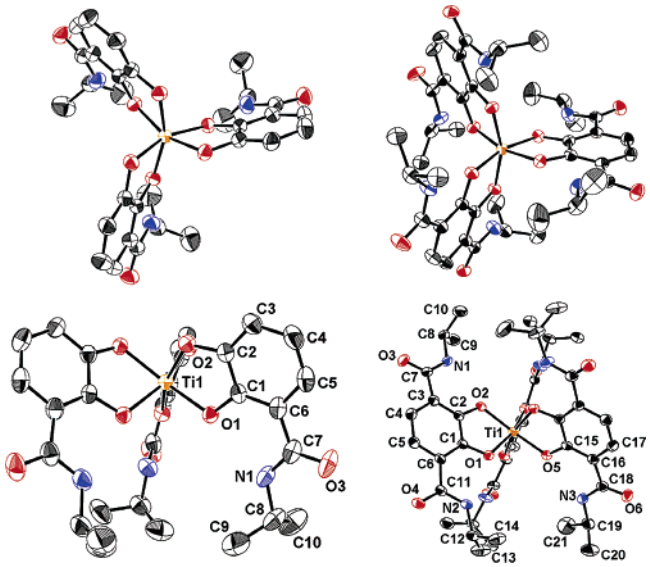

Figure 4. Left: ORTEP diagram of the Ti^{IV} complex from the $K_2[Ti\mathbf{1}_3]$·3DMF structure; space group $Pa\bar{3}$, a = 20.9569(8) Å, V = 9204.1(6) Å^3, Z = 8, R = 0.0546, R_w = 0.1506, GOF = 1.046. Right: ORTEP diagram of the Ti^{IV} complex from the $Na_2[Ti\mathbf{2}_3]$·5DMF structure; space group $C2/c$, a = 17.862(1) Å, b = 17.175(1) Å, c = 22.895(2) Å, β = 106.161(2)°, V = 6746.2(7) Å^3, Z = 4, R = 0.0552, R_w = 0.1385, GOF = 1.037. Hydrogen atoms have been omitted for clarity.

All four $Ti^{IV}L_3$ complexes are prepared from $TiO(acac)_2$, the respective ligand, and base. Weaker bases such as $NaHCO_3$ and $KHCO_3$ are employed to prevent base-dependent hydrolysis of the TiL_3 products.[32] Both the Na^+ and K^+ salts of complexes $[Ti\mathbf{1}_3]^{2-}$ and $[Ti\mathbf{2}_3]^{2-}$ crystallize readily with the diffusion of THF or ethyl acetate into DMF or ethanol to produce large orange-red crystals, and X-ray structures of $K_2[Ti\mathbf{1}_3]$ and $Na_2[Ti\mathbf{2}_3]$ were obtained (Figure 4).

The structures of both $[Ti\mathbf{1}_3]^{2-}$ and $[Ti\mathbf{2}_3]^{2-}$ reveal the expected tris-chelate complex. The tris-catecholamide complex $[Ti\mathbf{1}_3]^{2-}$ crystallized as the *fac* isomer in the cubic space group $Pa\bar{3}$ such that the complex has crystallographic three-fold symmetry. Crystallized in the monoclinic spacegroup $C2/c$, the

(28) Fortman, J. J.; Sievers, R. E. *Coord. Chem. Rev.* **1971**, *6*, 331−375.
(29) Kersting, B.; Meyer, M.; Powers, R. E.; Raymond, K. N. *J. Am. Chem. Soc.* **1996**, *118*, 7221−7222.
(30) Twist mechanisms (Bailar and Rây−Dutt) were also distinguished for the chemically similar $Os(DBQ)_3$ complex: ref 27.
(31) Rosenheim, A.; Sorge, O. *Chem. Ber.* **1920**, *53*, 932−939; Sau, A. C.; Holmes, R. R. *Inorg. Chem.* **1981**, *20*, 4129−4135.
(32) Borgias, B. A.; Cooper, S. R.; Koh, Y. B.; Raymond, K. N. *Inorg. Chem.* **1984**, *23*, 1009−1016.
(33) Parr, J.; Slawin, A. M. Z.; Woolins, J. D. *Polyhedron* **1994**, *13*, 3261−3263.
(34) Rosenheim, A.; Raibmann, B.; Schendel, G. *Z. Anorg. Allg. Chem.* **1931**, *196*, 160−176.

Table 1. $[TiL_3]^{2-}$ Structural Parameters

compound	distances Ti–O (Å)	bite angles (α) O–Ti–O (deg)	twist angle (*θ*) avg. (deg)	normalized bite (*b*)
$K_2[Ti\mathbf{1}_3]$	Ti1−O1 1.953(2) Ti1−O2 1.981(2)	O1−Ti1−O2 79.2(1)	36.3	1.27
$Na_2[Ti\mathbf{2}_3]$	Ti1−O1 1.948(2) Ti1−O2 1.962(2) Ti1−O5 1.954(2)	O1−Ti1−O2 79.3(1) O5−Ti1−O5* 78.8(1)	39.0	1.27
$(Et_3NH)_2[Ti(cat)_3]$[32]	1.941(1) 1.964(1) 1.933(1) 2.014(1) 1.986(1) 1.957(1)	80.6(1) 80.1(1) 80.3(1)	43.5	1.29

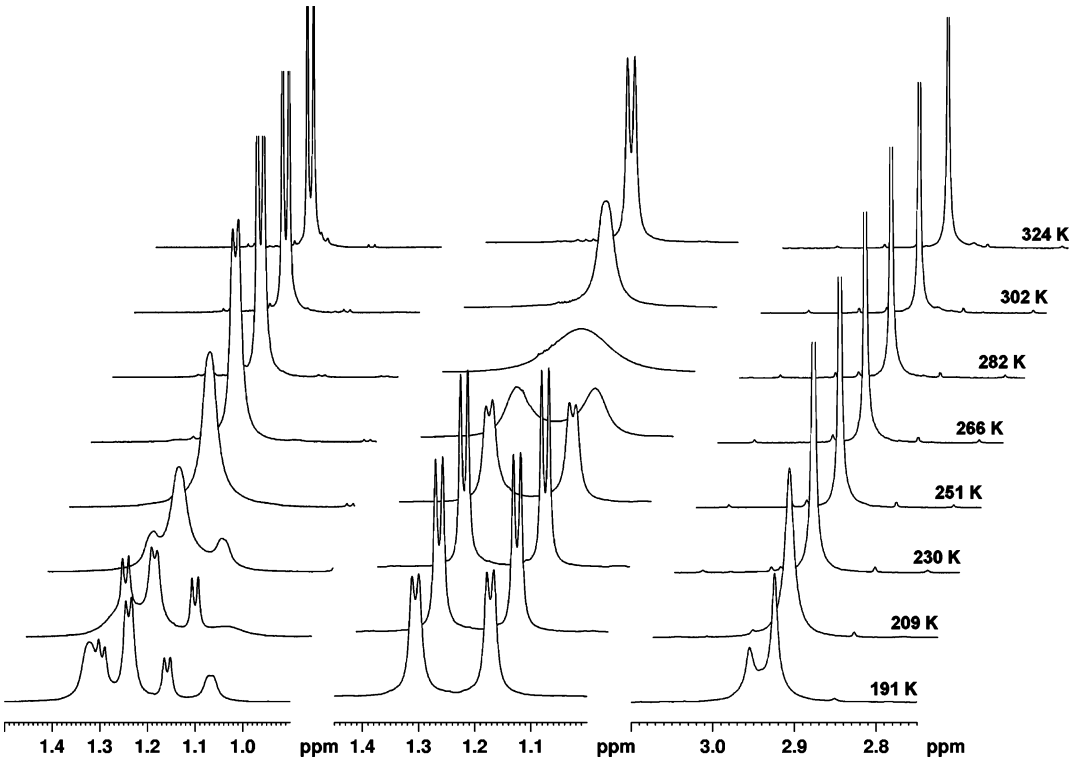

Figure 5. Aliphatic region of the VT ^{1}H NMR (500 MHz) spectra of $Na_2[Ti\mathbf{1}_3]$, $Na_2[Ti\mathbf{2}_3]$, and $Na_2[Ti\mathbf{3}_3]$ in methanol-d_4.

tris-terephthalamide complex $[Ti\mathbf{2}_3]^{2-}$ has crystallographic C_2 symmetry. A few relevant structural parameters for each complex are given in Table 1 and agree well with the reported $[Ti(cat)_3]^{2-}$ structure.[32] It should be noted that the normalized bites for each complex (1.27 and 1.27) lie close to Kepert's calculated boundary of 1.3 for the trigonal and rhombic twist mechanisms.[24]

^{1}H NMR study of $[Ti\mathbf{1}_3]^{2-}$, $[Ti\mathbf{2}_3]^{2-}$, and $[Ti\mathbf{3}_3]^{2-}$. ^{1}H NMR study of complexes $Na_2[Ti\mathbf{1}_3]$, $Na_2[Ti\mathbf{2}_3]$, and $Na_2[Ti\mathbf{3}_3]$ confirms Rosenheim's hypothesis of fast racemization. In fact, at room temperature, the spectrum of $[Ti\mathbf{1}_3]^{2-}$ in methanol-d_4 contains only one sharp isopropyl methyl resonance indicative of fast chemical exchange. Variable-temperature (VT) ^{1}H NMR spectra of all three Ti^{IV} complexes, recorded between 191 and 324 K in methanol-d_4, demonstrate the facile isomerization of all three complexes. The aliphatic regions of these spectra containing the methyl resonances of each complex are presented in Figure 5.

The spectra of $[Ti\mathbf{2}_3]^{2-}$ are straightforward to interpret. At the low-temperature limit (230 K) two sharp diastereotopic isopropyl methyl resonances are observed (Figure 5, middle), each coupled to the isopropyl methine. As the temperature increases, these resonances broaden and then coalesce—chemical exchange caused by racemization averages the two isopropyl methyl chemical environments. At the high temperature limit (324 K), only one sharp averaged isopropyl methyl resonance is observed. The terephthalamide aromatic protons remain chemically equivalent at all temperatures (Supporting Information).

The VT ^{1}H NMR spectra of $[Ti\mathbf{1}_3]^{2-}$ and $[Ti\mathbf{3}_3]^{2-}$ (Figure 5, left and right) show isomerization of the tris-catecholamide complexes. First, it is clear that the rate of isomerization of both tris-catecholamide species exceeds that of the tris-terephthalamide, making direct correlation of rate and mechanism among all three complexes uncertain. Only at the lowest temperature (191 K) is a second peak, corresponding to the meridional isomer, observed in the $[Ti\mathbf{3}_3]^{2-}$ spectrum. (If the facial complex were the only possible geometrical isomer, the spectrum should remain unchanged at all temperatures.) Three resonances are expected for the C_1 symmetric *mer* species, but

it is likely that these resonances are either very similar in chemical shift or that some are buried under the resonance of the *fac* isomer. In addition, a trigonal twist mechanism may average the symmetry of the *mer* isomer to C_s (Figure 1), causing two of the methyl groups to become chemically equivalent on the NMR time scale. (Further evidence for this process is discussed later with regard to the $[Ti\mathbf{1}_3]^{2-}$ and $[Ti\mathbf{4}_3]^{2-}$ complexes.) The *mer*⇌*fac* isomerization of $[Ti\mathbf{3}_3]^{2-}$ cannot occur by the trigonal twist—it must occur via the Rây−Dutt mechanism or a bond-rupture pathway.

The VT spectra of $[Ti\mathbf{1}_3]^{2-}$ (Figure 5, left) reveal the sensitivity of its ^{1}H NMR spectrum to both Δ⇌Λ and *mer*⇌*fac* isomerizations. Analogous to the $[Ti\mathbf{2}_3]^{2-}$ complex, two doublets are expected for the *fac* isomer, while six doublets should appear for a *mer* isomer. The spectra recorded at the lowest temperature (191 K) indicate that both isomers are present but have overlapping signals. The sharper signals at this temperature must correspond to a more intense pair of doublets for the *fac* isomer and one less intense pair of doublets for the *mer* isomer. The four other doublets of the *mer* isomer (again which overlap with the other resonances) remain broad at 191 K, indicating that the *mer* isomer is racemizing (Δ-*mer*⇌Λ-*mer*) faster than the *fac* isomer (Δ-*fac*⇌Λ-*fac*) and faster than the *mer* and *fac* isomers interconvert (Λ-*mer*⇌Δ-*fac* and Δ-*mer*⇌Λ-*fac*). By 230 K, when the signals of $[Ti\mathbf{2}_3]^{2-}$ are still sharp but those of $[Ti\mathbf{3}_3]^{2-}$ have already coalesced, the *mer* and *fac* isomers of $[Ti\mathbf{1}_3]^{2-}$ both demonstrate broadened resonances, indicative of their exchange.

The chemical differences between the tris-catecholamide and tris-dihydroxyterephthalamide complexes complicate comparison of the $[Ti\mathbf{1}_3]^{2-}$, $[Ti\mathbf{2}_3]^{2-}$, and $[Ti\mathbf{3}_3]^{2-}$ complexes. The donor oxygens of the tris-catecholamide ligands are electronically different, and the increased steric demand of the terephthalmide ligand, a disubstituted catechol, may be significant compared to that of the catecholamide, a monosubstituted catechol, in ML_3 intramolecular dynamics.[35] It is also of interest to make direct comparison of $[TiL_3]^{2-}$ isomerization to that reported for analogous $[GaL_3]^{3-}$ complexes.

The two principal gallium complexes used in previous studies of tris-catecholate racemization were based on ligands $H_2\mathbf{2}$ and $H_2\mathbf{4}$ (Figure 3), both dihydroxyterephthalamides derivatives. The choice of substituents for the unsymmetrical chelate $H_2\mathbf{4}$ is important for practical experimental reasons, as the benzyl and *tert*-butyl ^{1}H NMR resonances are in very different spectral regions. The *tert*-butyl groups are sensitive to only geometrical isomerism, while the benzyl methylene protons report both geometrical and stereoisomerism. Study of the Na_2- and $K_2[Ti\mathbf{2}_3]$ complexes in different solvents and at different concentrations was conducted to probe the relevance of bond-rupture pathways, while examination of the isomerization behavior of $K_2[Ti\mathbf{4}_3]$ assesses the contribution of *mer*⇌*fac* isomerization to the racemization process.

The Na_2 and K_2 salts of $[Ti\mathbf{2}_3]^{2-}$ produce identical VT ^{1}H NMR spectra in methanol-d_4, and spectra of $Na_2[Ti\mathbf{2}_3]$ at different concentrations were also indistinguishable. Coalescence of the ^{i}Pr methyl resonances due to $[Ti\mathbf{2}_3]^{2-}$ racemization occurs at 278.5 K in methanol-d_4 and at 296 K in DMF-d_7, corresponding to a difference of only 4 kJ/mol in $\Delta G^{\ddagger}$.[36,37] Line shape analysis[38,39] of the VT spectra of $K_2[Ti\mathbf{2}_3]$ in different solvents was performed to determine the rate of racemization at the temperature of each spectrum, and experimental and simulated spectra for the methanol-d_4 sample are shown in Figure 6.

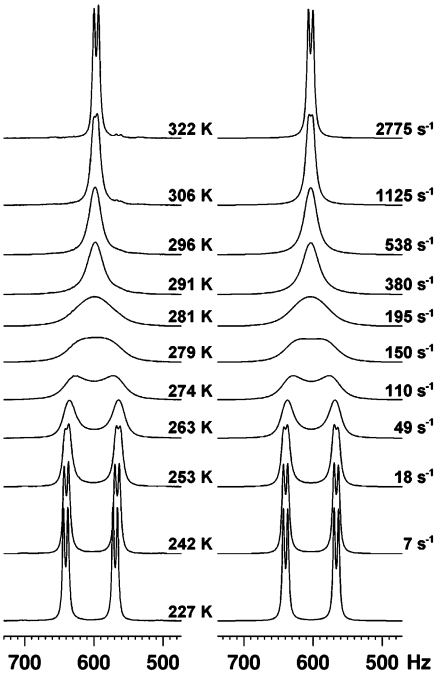

Figure 6. (Left) Experimental VT ^{1}H NMR (500 MHz) of $K_2[Ti\mathbf{2}_3]$ in methanol-d_4. (Right) Simulated spectra produced by line shape analysis.[38,39]

Table 2. Kinetic Parameters of $M2_3$ Racemization

solvent	$\Delta G^{\ddagger}_{298\ K}$ (kJ/mol)	$\Delta H^{\ddagger}$ (kJ/mol)	$\Delta S^{\ddagger}$ (J/molK)	$k_{298\ K}$ (s^{-1})
	$K_2[Ti\mathbf{2}_3]$			
methanol-d_4	57(3)	47(1)	−34(4)	630(10)
D_2O (pD* = 8.6) (20% MeOD)	56(3)	48(3)	−28(10)	840(40)
DMF-d_7	59(3)	55(1)	−16(4)	200(10)
	$K_3[Ga\mathbf{2}_3]$ (from ref 5)			
D_2O (pD = 7.2)	60(3)	46(2)	−47(5)	240(10)
D_2O (pD = 9.8)	66.8(6)	55.2(3)	−39(9)	11(1)
D_2O (pD = 12.1)	67.4(9)	58.5(6)	−30(9)	10(1)
DMSO-d_6	73(2)	67(1)	−20(10)	4(1)
DMSO-d_6 $(NMe_4)_3$ salt	75(2)	77(1)	0(10)	1(1)

Analysis of the variable-temperature racemization rates using Eyring theory allows for the determination of activation parameters, which can be compared to those determined for the $K_2[Ga\mathbf{2}_3]$ complex (Table 2). Racemization of the Ti^{IV} complex is clearly faster than that of the Ga^{III} complex. Furthermore, the small $\Delta H^{\ddagger}$ value and the small and negative $\Delta S^{\ddagger}$ values indicate an intramolecular mechanism which does not involve bond rupture. Comparable kinetic parameters were also found for the racemization of $K_2[Ti\mathbf{2}_3]$ in DMF-d_7 and buffered D_2O (pD = 8.6, 20% MeOD). That some solvent dependence of the

(35) Hay, B. P.; Dixon, D. A.; Vargas, R.; Garza, J.; Raymond, K. N. *Inorg. Chem.* **2001**, *40*, 3922−3935.

(36) Rate constants (k_c) at the coalescence temperature (T_c) can be calculated from the equation $k_c = 2.22\delta$, which produces 158 s^{-1} in methanol-d_4 (δ = 71 Hz) and 173 s^{-1} in DMF-d_7 (δ = 78 Hz) both in good agreement with the line shape analysis. The equation $\Delta G^{\ddagger} = 0.01913(10.13 + \log(T_c/k_c))$ then relates these values to inversion barrier estimations: $\Delta G^{\ddagger}_{MeOD}$ = 56 kJ/mol and $\Delta G^{\ddagger}_{DMF}$ = 60 kJ/mol, again in good agreement with line shape analysis results.

(37) Sandström, J. *Dynamic NMR Spectroscopy*; Academic Press Inc.: New York, 1982.

(38) Bain, A. D. *Mexico*, 2.0; 2001.

(39) Bain, A. D.; Duns, G. J. *Can. J. Chem.* **1996**, *74*, 3671−3653.

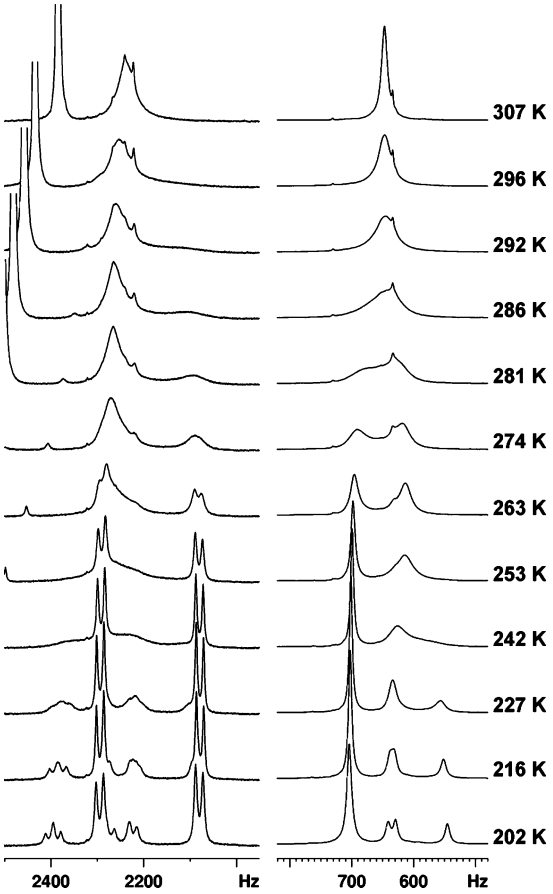

Figure 7. Benzyl CH_2 (left) and *tert*-butyl CH_3 (right) regions of the VT ^{1}H NMR (500 MHz) spectra of K_2[Ti**4**$_3$] in methanol-d_4.

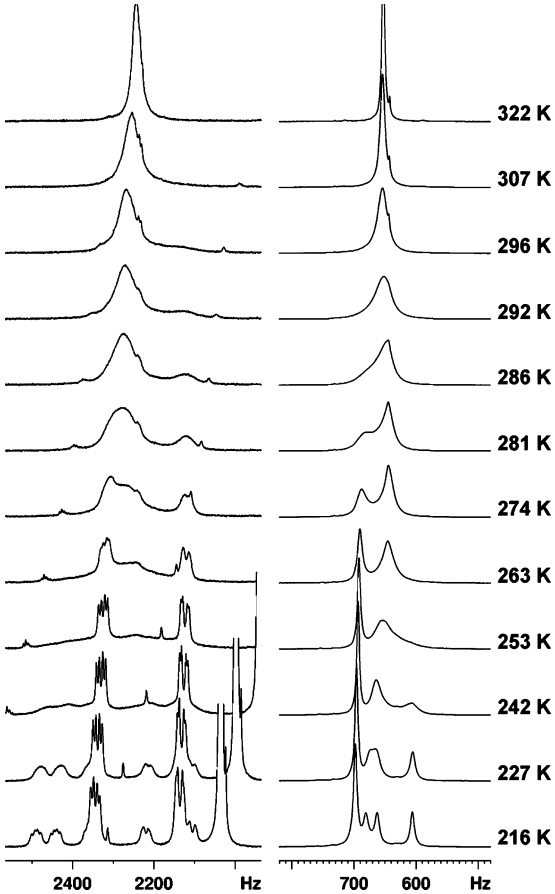

Figure 8. Benzyl CH_2 (left) and *tert*-butyl CH_3 (right) regions of the VT ^{1}H NMR (500 MHz) spectra of K_2[Ti**4**$_3$] in DMF-d_7. Coupling of the benzyl CH_2 protons to the amide N*H*, creates a more complex splitting pattern than was observed in the methanol-d_4 sample (Figure 7).

racemization rates is observed may be attributable to ion pairing and solvation differences in different solvents. (It was not possible to dissolve the complexes in water without the addition of methanol.) Ion pairing differences were also suggested in the Ga^{III} study, producing a T_c difference of 30 °C for the $[Ga\mathbf{2}_3]^{3-}$ complex in water versus DMSO.[5,40]

The kinetic parameters of $K_3[Ga\mathbf{2}_3]$ are also given in Table 2. At lower pH values the Ga^{III} racemization rate increases to values similar to those of Ti^{IV}. A proton-dependent (but nonbond-rupture) mechanism was described for pD values below 8. In the $K_2[Ti\mathbf{2}_3]$ case, proton dependence can be ruled out in the reported experiments. The pK_a of $H[Ti\mathbf{2}_3]^-$ is expected to be much lower than that of $H[Ga\mathbf{2}_3]^{2-}$,[41] and addition of NaOD to the $[TiL_3]^{2-}$ methanol-d_4 samples did not affect the observed line shapes at room temperature. Analogous VT ^{1}H NMR experiments were also conducted in methanol-d_4 in the presence of 4-(dimethylamino)pyridine (pK_a = 9.68, 25 °C)[42] and did not affect the observed $[Ti\mathbf{2}_3]^{2-}$line shapes at all temperatures.

The VT ^{1}H NMR spectra of the $K_2[Ti\mathbf{4}_3]$ complex contribute to the development of a racemization mechanism. These spectra are presented in Figure 7, and the patterns of spectral change again mirror what was observed for the Ga^{III} analogue but occur at lower temperature due to the faster rates of Ti^{IV} isomerization.

As observed for the $[Ga\mathbf{4}_3]^{3-}$ complex, four *tert*-butyl CH_3 resonances are observed at the low-temperature limit (209 K) in methanol-d_4 (Figure 7, right) and in DMF-d_7 (Figure 8, right) one corresponding to the C_3 symmetric *fac* complex (700 Hz) and three at higher field corresponding to the C_1 symmetric *mer* complex. At low temperature, the *fac*:*mer* ratio is approximately 4:3 in methanol-d_4 and 1:1 in DMF-d_7, both higher than the statistically predicted 1:3 ratio.[43] As the temperature is raised, broadening and coalescence of two of the three *mer* resonances occurs ($T_c \approx 242$ K, $\delta = 95$ Hz, $k_c = 211$ s^{-1}, $\Delta G^{\ddagger} = 48$ kJ/mol) before broadening of the *fac* resonance. The same process occurs in DMF-d_7 (Figure 8) but at a slightly higher temperature ($T_c \approx 253$ K, $\delta = 74$ Hz, $k_c = 164$ s^{-1}, $\Delta G^{\ddagger} = 51$ kJ/mol), producing the same estimated solvent dependent difference in $\Delta G^{\ddagger}$ as was observed for $[Ti\mathbf{2}_3]^{2-}$. The two coalescing *mer* CH_3 groups are averaged by a Bailar mechanism faster than they are exchanged with the *fac* CH_3 groups by a Rây−Dutt mechanism, an observation again paralleling the Ga^{III} study. As was illustrated in Figure 1, the Bailar twist can only interconvert enantiomers, not geometrical isomers.

(40) Recent studies of the Li^+ salts of Ga^{III} and Ti^{IV} tris-catecholate complexes demonstrate their propensity to form cation-linked structures, further supporting the existence of significant ion-pairing interactions: Albrecht, M.; Mirtschin, S.; de Groot, M.; Janser, I.; Runsink, J.; Raabe, G.; Kogej, M.; Schalley, C.; Frohlich, R. *J. Am. Chem. Soc.* **2005**, *127*, 10371−10387.

(41) Preliminary titrations of a $[TiL]^{2-}$ hexadentate catecholamide complex indicate that the highest catecholate pK_a is well below 3 compared to a value of 4.5 for a comparable Ga^{III} complex; Loomis, L. D.; Raymond, K. N. *Inorg. Chem.* **1991**, *30*, 906−911.

(42) Bunting, J. W.; Stefanidis, D. *J. Am. Chem. Soc.* **1990**, *112*, 779−786.

(43) The *fac*:*mer* ratio for the $[Ga\mathbf{4}_3]^{2-}$ was reported to be 0.78 in both DMSO-d_6 and D_2O. For both the Ti^{IV} and Ga^{III} complexes, this ratio clearly changes in the temperature range in which *mer*⇌*fac* isomerization broadens the ^{t}Bu resonances in all solvents.

Table 3. $[GeL_3]^{2-}$ Structural Parameters

compound	distances Ge–O (Å)	bite angles (α) O–Ge–O (deg)	twist angle (θ) avg. (deg)	normalized bite (*b*)
$K_2[Ge\mathbf{2}_3]$	Ge1−O1 1.886(2) Ge1−O2 1.880(2) Ge1−O5 1.885(2) Ge1−O6 1.874(2) Ge1−O9 1.889(2) Ge1−O10 1.876(2)	O1−Ge1−O2 85.0(1) O5−Ge1−O6 85.3(1) O9−Ge1−O10 85.2(1)	50.2	1.35
$K_2[Ge(cat)_3]$[33]	1.894(5) 1.874(5) 1.905(4) 1.903(5) 1.901(5) 1.890(4)	86.9(2) 86.4(2) 87.0(2)	52.7	1.37

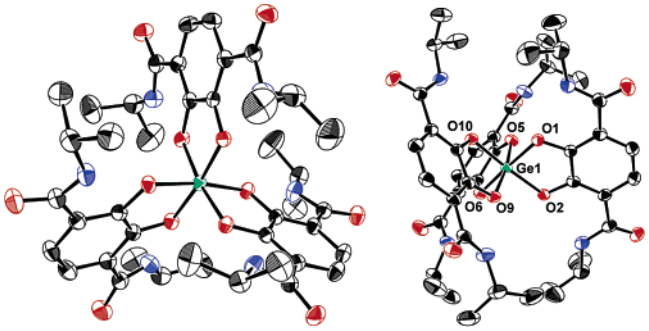

Figure 9. ORTEP diagram of the Ge^{IV} complex from the crystal structure of $K_2[Ge\mathbf{2}_3]\cdot 4C_3H_6O$: space group $P\bar{1}$, $a = 12.4117(14)$ Å, $b = 13.7070(15)$ Å, $c = 19.505(2)$ Å, $\alpha = 89.074(2)°$, $\beta = 75.986(2)°$, $\gamma = 80.030(2)°$, $V = 3169.9(6)$ Å^3, $Z = 2$, $R = 0.0586$, $R_w = 0.1654$, GOF = 1.068. Hydrogen atoms have been omitted for clarity. (Full numbering of the complex is presented in the Supporting Information section.)

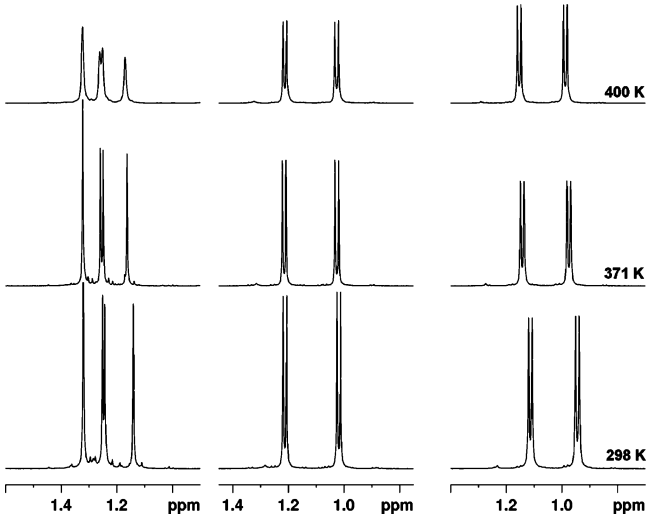

Figure 10. VT ^{1}H NMR (500 MHz) spectra of $K_2[Ge\mathbf{4}_3]$ (left, *fac* and *mer* ^{t}Bu resonances, DMF-d_7) and $K_2[Ge\mathbf{2}_3]$ (^{i}Pr resonances: middle, DMF-d_7; right, DMSO-d_6). The slight broadness of the $K_2[Ge\mathbf{4}_3]$ spectrum at 400 K may be due to shimming difficulty for DMF-d_7 at high temperature.

Further information is gleaned from examination of the benzyl CH_2 resonances, as the two methylene protons are diastereotopic. The two distinct doublets of the *fac* isomer remain sharp as the two *mer tert*-butyl CH_3 resonances coalesce and as the *mer* benzyl CH_2 resonances broaden. Only at higher temperature (263 K, methanol-d_4 and DMF-d_7) do the two benzyl CH_2 doublets of the *fac* complex begin to broaden. It is not possible to analyze the racemization of the *fac* isomer, however, as *fac*⇌*mer* interconversion begins in the same temperature range, as indicated by the broadening of the *fac* ^{t}Bu resonance and its subsequent coalescence (281 K, methanol-d_4; 286 K DMF-d_7) with the averaged *mer* ^{t}Bu resonances. Therefore, if the trigonal twist is operative for the *fac*-$[Ti\mathbf{4}_3]^{2-}$ isomer, it must occur at a rate approximately equal to or slower than that of the Ray−Dutt *fac*⇌*mer* interconversion. The relationships between the relative isomerization processes of *mer* and *fac* isomers are thus the same for Ti^{IV} as were reported for Ga^{III}. However, the Ti^{IV} complexes undergo all intramolecular isomerizations faster than the Ga^{III} complexes.

Tris-catecholate Ge^{IV} Complexes. The rearrangement dynamics of Ge^{IV} tris-catecholate complexes were investigated to compare the behavior of the d^0 Ti^{IV} species to that of a d^{10} metal ion of the same oxidation state. The $K_2[Ge\mathbf{2}_3]$ and $K_2[Ge\mathbf{4}_3]$ complexes are prepared from $Ge(O^iPr)_4$ following procedures similar to those reported for the Ti^{IV} analogues. Crystals of the complex grew from a solution of ethanol with the diffusion of acetone, and the X-ray crystal structure of the complex was obtained (Figure 9).

The $[Ge\mathbf{2}_3]^{2-}$ structure possesses the anticipated tris-chelate coordination with the larger twist angle expected for a metal ion of smaller radius and shorter M−O bond lengths.[24,44] The structural parameters of the complex match those observed for the reported $[Ge(cat)_3]^{2-}$ structure and are summarized in Table 3.

Variable-temperature ^{1}H NMR study of the $K_2[Ge\mathbf{2}_3]$ and $K_2[Ge\mathbf{4}_3]$ complexes reveals the extreme inertness of these complexes to isomerization compared to their Ga^{III} and Ti^{IV} analogues (Figure 10). No broadening of the spectra of $K_2[Ge\mathbf{2}_3]$ is observed in DMF-d_7 or DMSO-d_6 at temperatures as high as 400 K. It is unclear if the apparent broadening of the ^{t}Bu resonances of $K_2[Ge\mathbf{4}_3]$ at 400 K reflects the onset of isomerization or merely the experimental difficulty encountered in shimming the DMF-d_7 sample at this temperature.

The solution behavior of the Ge^{IV} complexes supports the observation that isomerization of the d^{10} complexes is slower than that of the d^0 Ti^{IV} analogues. The Ti^{IV} results can be compared with both those of Ge^{IV}, an isovalent d^{10} ion, and those of Ga^{III}, which is more similar to Ti^{IV} in ionic radius and generates complexes of similar bite and twist angles.

Transition Metal Stabilization of Nonoctahedral Coordination Geometries. The Bailar and Rây−Dutt twist mechanisms are invoked in describing the intramolecular isomerization of both Ga^{III} and Ti^{IV} tris-catecholate complexes with the Ti^{IV}

(44) Borgias, B. A.; Barclay, S. J.; Raymond, K. N. *J. Coord. Chem.* **1986**, *15*, 109−123.

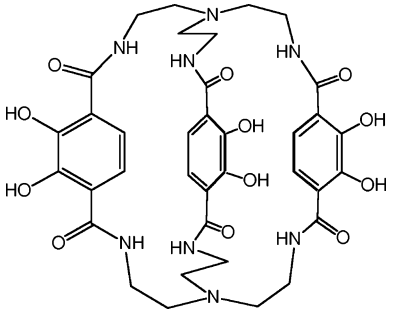

Figure 11. Macrobicyclic ligand H_6**A** is predisposed for trigonal prismatic coordination.[48]

compounds undergoing all rearrangements faster than the Ga^{III} and Ge^{IV} compounds.[8,28,32,45,46] These observations imply that the respective D_{3h} and C_{2v} transition-state structures of the Ti^{IV} complexes are energetically more accessible than the corresponding Ga^{III} and Ge^{IV} transition-state structures. In the past two decades, the significance of the D_{3h} trigonal prismatic coordination geometry in particular has garnered considerable attention in the chemistry of early transition metal complexes (especially that of d^0 ions). These findings are of relevance to the current studies.

The greater accessibility of the trigonal prismatic geometry for transition metal tris-catecholate complexes with empty or partially filled 3d orbitals is supported by previous structural studies.[47,48] The macrobicyclic tris-terephthalamide ligand H_6**A** (Figure 11), chemically very similar to the ligands used here, is predisposed to form trigonal prismatic complexes, as demonstrated by the "relaxed" conformation observed in a crystal structure of the free ligand. Octahedral M**A** coordination induces strain as the ligand is forced to twist. Indeed the crystal structures of three transition metal M**A** complexes (Ti^{IV}, V^{IV}, and Fe^{III}) show trigonal prismatic coordination ($\theta = 0-11.2°$). Structures of M**A** complexes with d^{10} ions (Al^{III} and Ga^{III}) exhibit the pseudooctahedral coordination polyhedra anticipated for the unconstrained tris complexes ($\theta = 40.3°$, 34.2°).

The trigonal prismatic (TP) coordination geometry is not predicted by the standard model of the valence shell electron pair repulsion theory (for d^2sp^3 hybridization); octahedral coordination best minimizes the repulsion of six-point charges (ligands) around a central metal ion. The absence of known trigonal prismatic structures was itself thought to be evidence of the inaccessibility of the TP coordination geometry.[49] However, d orbital involvement in metal−ligand bonding can change this picture.

On the basis of symmetry and molecular orbital arguments, Hoffmann and co-workers proposed in 1976 that a possible preference for TP geometries exists in transition metal compounds with few d electrons.[50] For transition metal complexes with energetically low-lying d orbitals, they reasoned that the trigonal prism allows all d orbitals to participate in σ bonding. This study also recognized the significance of the energetic accessibility of the TP to the barrier of the trigonal twist; thus, Hoffmann all but explicitly predicted a difference in twist rates for d^0 and d^{10} metal ions.

Later predictions that octahedral coordination is unstable for certain alkyl and hydride complexes of d^0 metals are now well-known.[51,52] The argument is made that strong σ donor ligands such as H^- and CH_3^- promote a second-order Jahn−Teller distortion leading to the mixing of t_{1u} HOMO and t_{2g} LUMO orbitals and stabilization of D_{3h} or C_{3v} coordination geometries.[52] Landis and co-workers made similar predictions based on their extension of Linus Pauling's valence bond theory, showing that sd^5 hybridization in WH_6 and $W(CH_3)_6$ leads to C_{3v} distorted trigonal prismatic coordination.[53] Crystal structures of $[Zr(CH_3)_6]^{2-}$,[54] $W(CH_3)_6$ and $Re(CH_3)_6$,[55] as well as DFT-corroborated infrared observation of WH_6 in a neon matrix,[27] validate these calculations and emphasize the contribution of d orbitals to covalent transition metal bonding and structure.

It is often stressed that trigonal prismatic distortion is favored by strong σ donor ligands with little π-donating capability, yet recent calculations point to more broadly reaching effects of d orbital involvement in transition metal bonding.[56] The difference in energy between the TP and octahedral geometries of WCl_6 is calculated to be 80 kJ/mol. Replacement of one Cl^- by a CH_3^- lowers the energy difference to 20 kJ/mol, whereas the energy difference vanishes for the $W(CH_3)_2Cl_4$ compound. The weaker π-donor character of F^- already contributes to a calculated energy difference of only 43 kJ/mol for the TP and octahedral forms of WF_6.

Finally, π-bonding arguments have also been made in describing the stabilization of TP geometries.[50,57] Critical to the current study, rigorous spectroscopic analysis of the electronic structure of $[Fe(cat)_3]^{3-}$ complexes identified significant π contributions to the Fe−O bonding which can be evaluated from details of the complexes' charge-transfer spectra.[58] Extension of this work to studies of the [Fe**A**]$^{3-}$ and [V**A**]$^{2-}$ complexes indicated that ligand-to-metal π bonding is in fact maximized in the TP structures (and actually greater for the d^1 V^{IV} complex than for the d^5 Fe^{III} complex) and therefore responsible for the observed coordination geometry of the transition metal M**A** complexes.[48] Spectra of the Ti^{IV} analogues are significantly different and could not be interpreted in the same manner,

(45) It should be noted that extensive study of $Ti(acac)_2(OR)_2$- and $Ti(acac)_2X_2$-type complexes has also demonstrated the facile intramolecular rearrangement of Ti^{IV} species and comparison to Ga^{III} and Ge^{IV} complexes reveals the same rate relationship among the three metals as is found here. Nonrupture twist mechanisms are often invoked, particularly for the $Ti(acac)_2(OR)_2$ complexes; Fay, R. C. *Coord. Chem. Rev.* **1996**, *154*, 99−124; Fay, R. C.; Lindmark, A. F. *J. Am. Chem. Soc.* **1983**, *105*, 2118−2127; Bradley, D. C.; Holloway, C. E. *J. Chem. Soc. (A)* **1969**, 282−285.

(46) It is acknowledged that the contribution of bond-rupture pathways cannot be completely ruled out on the basis of the current study, although our experience with Ti^{IV} and Ge^{IV} tris-catecholate complexes indicates that they are less labile than Ga^{III} analogues: Davis, A. V.; Raymond, K. N. *J. Am. Chem. Soc.* **2005**, *127*, 7912−7919; and ref 32.

(47) McMurry, T. J.; Hosseini, M. W.; Garrett, T. M.; Hahn, F. E.; Reyes, Z. E.; Raymond, K. N. *J. Am. Chem. Soc.* **1987**, *109*, 7196−7198.

(48) Karpishin, T. B.; Stack, T. D. P.; Raymond, K. N. *J. Am. Chem. Soc.* **1993**, *115*, 182−192.

(49) Muetterties, E. L. *J. Am. Chem. Soc.* **1968**, *90*, 5097−5102.

(50) Hoffmann, R.; Howell, J. M.; Rossi, A. R. *J. Am. Chem. Soc.* **1976**, *98*, 2484−2492.

(51) Demolliens, A.; Jean, Y.; Eisenstein, O. *Organometallics* **1986**, *5*, 1457−1464; Shen, M.; Schaefer, H. F., III; Partridge, H. *J. Chem. Phys.* **1993**, *98*, 508−521; Kwang, S. K.; Tang, H.; Albright, T. A. *J. Am. Chem. Soc.* **1993**, *115*, 1971−1981.

(52) Kwang, S. K.; Albright, T. A.; Eisenstein, O. *Inorg. Chem.* **1989**, *28*, 1611−1613.

(53) Landis, C. R.; Cleveland, T.; Firman, T. K. *J. Am. Chem. Soc.* **1995**, *117*, 1859−1860.

(54) Morse, P. M.; Girolami, G. S. *J. Am. Chem. Soc.* **1989**, *111*, 4114−4116.

(55) Pfennig, V.; Seppelt, K. *Science* **1996**, *271*, 626−628.

(56) Kaupp, M. *Angew. Chem., Int. Ed.* **1999**, *38*, 3034−3037; Kaupp, M. *Angew. Chem., Int. Ed.* **2001**, *40*, 3534−3565.

(57) Comba, P.; Sargeson, A. M.; Engelhardt, L. M.; Harrowfield, J. M.; White, A. H.; Horn, E.; Snow, M. R. *Inorg. Chem.* **1985**, *24*, 2325−2327; Stiefel, E. I.; Eisenberg, R.; Rosenberg, R. C.; Gray, H. B. *J. Am. Chem. Soc.* **1966**, *88*, 2956−2966.

(58) Karpishin, T. B.; Gebhard, M. S.; Solomon, E. I.; Raymond, K. N. *J. Am. Chem. Soc.* **1991**, *113*, 2977−2984.

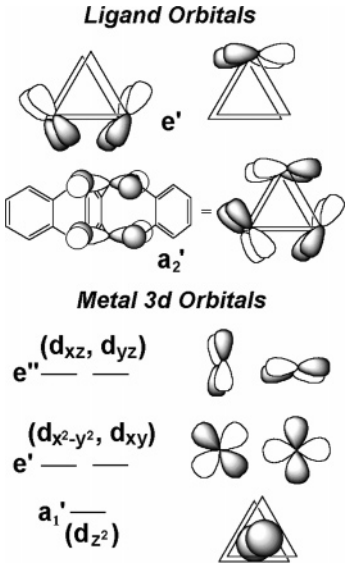

Figure 12. For D_{3h}-symmetric M(cat)$_3$ complexes, the six catecholate π-bonding orbitals transform as A$_2$′, E′, A$_1$″, and E″. The a$_1$″ and e″ orbitals differ from their a$_2$′ and e′ counterparts by being anti-symmetric with respect to the horizontal mirror plane (σ_h, in the plane of the page). The HOMO of catechol itself is C_2-symmetric (i.e. as drawn in the a$_2$′ and e′ sets above). Analysis of the ligand and metal orbitals for the D_3 symmetric ground state of M(cat)$_3$ complexes, produces similar results. (The absence of the σ_h operation in the D_3 point group obviates the ′ and ″ designations.) The metal e″ orbital set correlates to the e$_g$ set (d$_{z^2}$, d$_{x^2-y^2}$) of the more familiar O_h ligand field, while both the a$_1$′ and e′ sets correlate to the t$_{2g}$ (d$_{xy}$, d$_{xz}$, d$_{yz}$) of the O_h ligand field. (The lowering of symmetry from O_h to D_3 or D_{3h} results in a change in axes and thus a change in labels for the d orbitals.)

although it seems likely that the same π-bonding effect is also operative in the TP [Ti**A**]$^{2-}$ complex. Ligand orbitals relevant to π interactions in the D_{3h} TP configuration are depicted in Figure 12 along with representations of the metal 3d orbitals. It is the π interaction of the catecholate orbitals which was identified as being responsible for the accessibility of the TP geometry of the transition metal M**A** complexes.

DFT Calculation of ML$_3$ Stereoinversion Barriers. Density functional theory (DFT) calculations were conducted to evaluate the relative contributions of the Rây−Dutt and Bailar mechanisms in the stereoinversion of Ga^{III}, Ti^{IV}, and Ge^{IV} tris-catecholate complexes. These calculations also probe the predicted effect of each metal ion on the isomerization processes. To simplify the calculations, tris-2,3-dihydroxy-*N*,*N*′-dimethyl-terephthalamide complexes (M**B**$_3$) were modeled in place of the tris-diisopropyl-substituted M**2**$_3$ complexes used in the experimental studies. Calculations were also performed on the tris-catecholate complexes (M(cat)$_3$) of each metal, and ground state and transition-state geometries for all complexes were optimized using density functional theory.

Three configurations were calculated for each of the six metal complexes ([Ga(cat)$_3$]$^{3-}$, [Ga**B**$_3$]$^{3-}$, [Ti(cat)$_3$]$^{2-}$, [Ti**B**$_3$]$^{2-}$, [Ge(cat)$_3$]$^{2-}$, and [Ge**B**$_3$]$^{2-}$): the D_3 pseudo-octahedral ground state, the D_{3h} trigonal prism transition state of the Bailar twist and the C_{2v} transition state of the Rây−Dutt twist. Frequency calculations establish that the pseudooctahedral configurations are true minima (no negative frequencies) and that the D_{3h} and C_{2v} configurations are first-order transition states (one negative frequency). The optimized geometries are shown for [Ga(cat)$_3$]$^{3-}$ (Figure 13). Geometric parameters and relative energies are summarized in Table 4.

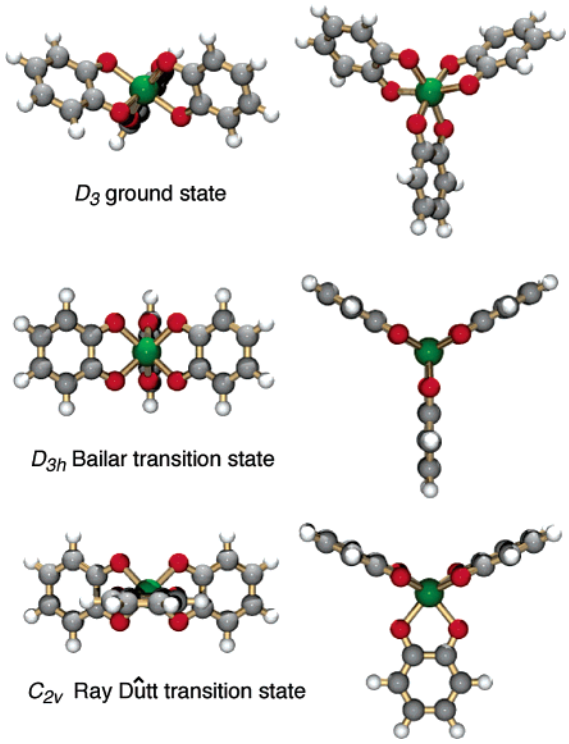

Figure 13. Optimized geometries for calculated D_3, D_{3h}, and C_{2v} configurations of [Ga(cat)$_3$]$^{3-}$.

A comparison of the calculated geometries with those observed in crystal structures reveals that this level of theory provides a relatively accurate prediction of structure. The experimental M−O bond lengths are systematically overestimated by an average of 0.03 Å. Bites (O−O distances) are reproduced with an average discrepancy of ±0.02 Å, and twist angles are reproduced to within ±2°.

For all six complexes, the Bailar twist D_{3h} transition-state configuration is calculated to be lower in energy than the C_{2v} transition-state configuration of the Rây−Dutt mechanism; yet the difference in energy between the two transition-state configurations is small (approximately 13 kJ, or 3 kcal) for all complexes. This relationship agrees with the experimentally observed behavior of the [Ti(**1**−**3**)$_3$]$^{2-}$ series, and of the [Ga**4**$_3$]$^{3-}$ and [Ti**4**$_3$]$^{2-}$ complexes for which the Bailar twist of the meridional isomers was found to be faster than the Rây−Dutt interconversion of facial and meridional isomers.[5] It should be noted that previously reported MM3 computational studies of the racemization of [Ga**2**$_3$]$^{3-}$ suggest that its relative steric congestion compared to [Ga(cat)$_3$]$^{3-}$ increases the trigonal twist barrier.[35,59]

The experimental findings from the M**4**$_3$ complexes demonstrate that the decreased steric congestion of the *mer* isomer relative to the *fac* isomer leads to a faster Bailar twist for the *mer* complex. Further, the data support the hypothesis that the Rây−Dutt mechanism becomes energetically more competitive (or even favorable) for more congested complexes, such as the *fac*-M**4**$_3$ species.

The calculations also correctly predict the relative rates of isomerization of the Ga^{III}, Ti^{IV}, and Ge^{IV} complexes, with Ti^{IV}

(59) In addition, simultaneous rotation of one or more isopropyl groups was indicated, implying that a number of possible trigonal prismatic transition states might be equally accessible and might severely complicate the calculation.

Table 4. Calculated Energies and Structural Parameters for ML_3 Complexes (experimental values in parentheses)[a]

	$[Ti(cat)_3]^{2-}$ (ref 32)	$[Ti(\mathbf{B})_3]^{2-}$	$[Ga(cat)_3]^{3-}$ (ref 44)	$[Ga(\mathbf{B})_3]^{3-}$ (ref 60)	$[Ge(cat)_3]^{2-}$ (ref 33)	$[Ge(\mathbf{B})_3]^{2-}$
			D_3 Ground State			
M−O (Å)	2.000	1.987	2.032	2.006	1.934	1.917
	(1.97)	1.96)	(1.98)	(1.97)	(1.89)	(1.88)
O−O (Å)	2.544	2.508	2.656	2.604	2.618	2.577
(chelate bite)	(2.54)	(2.47)	(2.65)	(2.57)	(2.60)	(2.54)
normalized	1.27	1.26	1.31	1.30	1.35	1.34
bite, *b*	(1.29)	(1.27)	(1.34)	(1.30)	(1.37)	(1.35)
twist, θ (deg)	41.5	39.9	47.8	45.9	51.9	50.4
	(43)	(39)	(49)	(44)	(53)	(50)
			D_{3h} Bailar Twist Transition State			
ΔE, kJ/mol	**36**	**39**	**53**	**53**	**95**	**96**
M−O, Å	2.001	1.998	2.063	2.035	1.973	1.954
			C_{2v} Rây−Dutt Twist Transition State			
ΔE, kJ/mol	**51**	**51**	**67**	**67**	**107**	**106**
$M-O_a$	1.996	1.990	2.048	2.027	1.959	1.945
$M-O_b$	2.031	2.008	2.089	2.048	1.997	1.969
$\Delta H^{\ddagger}$ observed ($M2_3$), kJ/mol		**47−55**		**55−77**		**N/A**

[a] In the C_{2v} structure, $M-O_a$ refers to the four identical bonds and $M-O_b$ refers to the two identical bonds. Experimental values (in parentheses) are taken from crystal structures. Experimental values for $M\mathbf{B}_3$ terephthalamide complexes are from the structures of $[Ti(\mathbf{2})_3]^{2-}$ and $[Ge(\mathbf{2})_3]^{2-}$ and a Ga^{III} tris(*N*,*N*′-bis((*S*)-α-methylbenzyl)-2,3-dihydroxyterephthalamide complex.[60]

giving the lowest activation barriers and Ge^{IV} the highest. That the Ga^{III} and Ti^{IV} barriers are closer in energy to one another than either is to the Ge^{IV} barriers also agrees with the experimental data. Comparing the calculation results for the simple catecholate ligands with those of the amide-substituted catecholate ligands reveals that the presence of *N*-methylamide groups does not significantly influence the barrier heights. As anticipated, however,[35] the calculated barriers are lower than the experimental values obtained when *N*-isopropylamide substituents are present.

For a given ligand, the Kepert model predicts that the barriers to rearrangement should increase as the metal−ligand bond lengths decrease.[24] If the ligand bite (i.e. the catechol O−O distance) were constant, then the normalized bite (d_{O-O}/d_{M-O}) would be inversely proportional to the M−O distance and the barriers to rearrangement should increase as the M−O distance decreases. Assuming a constant bite and taking the experimental tris-catecholate M−O distances of 1.97 Å (Ti^{IV}), 1.98 (Ga^{III}), and 1.89 (Ge^{IV}) correctly predicts that Ge^{IV} should exhibit higher barriers than the other two metals, but *incorrectly* predicts that Ti^{IV} should exhibit a barrier slightly lower than that of Ga^{III}.[61]

The data in Table 4 show that the catecholate bite in the tris-catecholate complexes exhibits significant variation. In the D_3 ground states the bites are 2.54 Å (Ti^{IV}), 2.65 Å (Ga^{III}), and 2.62 Å (Ge^{IV}). Examination of crystal structure data for all known tris-catecholate complexes[32,33,44,62] provides a basis for understanding the source of the bite variation. A plot of bite versus M−O distance (Figure 14) reveals that the catecholate bite is indeed quite variable, ranging from a minimum of 2.45 Å with P^V to a maximum of 2.71 Å with Sn^{IV}. The main group elements exhibit a smooth trend of increasing bite with increasing M−O distance. Of the five transition metal examples,

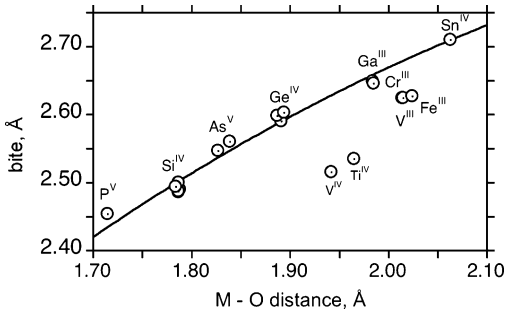

Figure 14. Plot of the bite versus the average M−O distance taken from 18 crystal structure examples of tris-catecholate complexes containing unsubstituted catecholate ligands.[32,33,44,62] The curve illustrates the smooth trend exhibited by the main group elements.

Table 5. Angular Preferences for Covalent Transition Metal Bonding[53]

metal	available orbitals	preferred bite angles
Ti^{IV}	sd^5	63, 117
V^{IV}	sd^4	66, 114
V^{III}	sd^3	71, 109
Cr^{III}	sd^2	90
	sd	90
Fe^{III}	s	none

only Cr^{III} follows the trend of the main group elements. The bites in the other transition metal complexes are smaller than those of similarly sized main group elements. The decrease in bite is most pronounced for Ti^{IV} and V^{IV}. The aberrant behavior of the transition metals can be rationalized by considering differences in the covalent contributions to the bonding.

(60) Karpishin, T. B.; Stack, T. D. P.; Raymond, K. N. *J. Am. Chem. Soc.* **1993**, *115*, 6115−6125.

(61) The significant deviation in catechol bite for the Ti^{IV} catecholate complexes is unexpected for a rigid chelate, as described. We note that because of this bite deviation, the isomerization rates for the Ti^{IV}, Ga^{III}, and Ge^{IV} complexes do follow the normalized bite (*b*) trend. However, the normalized bite trend is not established by the progression of metal−ligand bond lengths or of ionic radii, as the Kepert model assumes. Rather, it is precisely due to the differences in metal−ligand bonding described here.

(62) Tacke, R.; Stewart, A.; Becht, J.; Burschka, C.; Richter, I. *Can. J. Chem.* **2000**, *78*, 1380−1387; Allcock, H. R.; Bissell, E. C. *J. Am. Chem. Soc.* **1973**, *95*, 3154−3157; Bindu, P.; Varghese, B.; Rao, M. N. S. *Phosphorus, Sulfur Silicon Relat. Elem.* **2003**, *178*, 2373−2386; Flynn, J. J.; Boer, F. P. *J. Am. Chem. Soc.* **1969**, *91*, 5756−5761; Kobayashi, R.; Ito, T.; Marumo, F.; Saito, Y. *Acta Crystallogr., Sect. B* **1972**, *28*, 3446−3451; Borgias, B. A.; Hardin, G. G.; Raymond, K. N. *Inorg. Chem.* **1986**, *25*, 1057−1060; Cooper, S. R.; Koh, Y. B.; Raymond, K. N. *J. Am. Chem. Soc.* **1982**, *104*, 5092−5102; Raymond, K. N.; Isied, S. S.; Brown, L. D.; Fronczek, F. R.; Nibert, J. H. *J. Am. Chem. Soc.* **1976**, *98*, 1767−1773; Anderson, B. F.; Buckingham, D. A.; Robertson, G. B.; Webb, J. *Acta Crystallogr., Sect. B* **1982**, *38*, 1927−1931; Holmes, R. R.; Shafieezad, S.; Chandrasekhar, V.; Sau, A. C.; Holmes, J. M.; Day, R. A. *J. Am. Chem. Soc.* **1988**, *110*, 1168−1174.

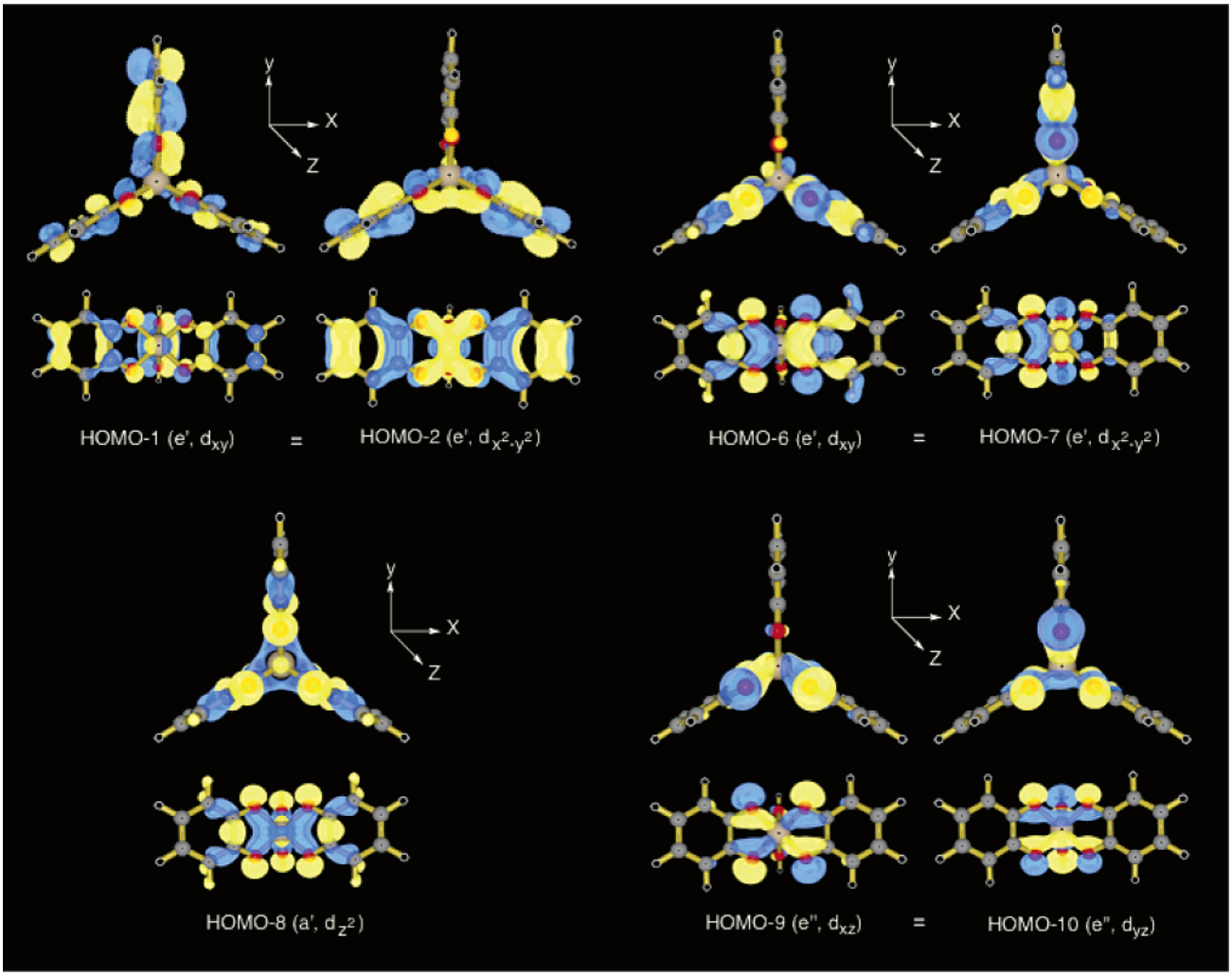

Figure 15. Graphical representation of the $[Ti(cat)_3]^{2-}$ molecular orbitals, illustrating d-orbital involvement in the D_{3h} Bailar twist transition state. Percent d orbital contribution for each set of orbitals is: HOMO−1 and −2 (4.9% d_{xy}, $d_{x^2-y^2}$, π interaction), HOMO−6 and −7 (6.2% d_{xy}, $d_{x^2-y^2}$, σ interaction), HOMO−8 (2.7% d_{z^2}, σ interaction), and HOMO−9 and −10 (8.1% d_{xz} d_{yz}, σ interaction).

First consider the ionic limit in which there is no directionality at the metal center. In the absence of covalent interactions, the bite will be influenced by interligand steric repulsion. As the coordination sphere contracts, the repulsion increases and is relieved by decreasing the bite. Thus, there should be a tendency toward smaller bite with smaller metal size, and this general tendency is observed in the data.

In contrast, covalent bonding contributions give rise to metal-centered directionality that can be described in terms of preferred bite angles, in this case O−M−O angles. For the main group elements, where bonding involves s and p orbitals, any covalent contribution favors bite angles ≥90°. The smooth trend observed for the main group elements (Figure 14) is consistent with an identical bite angle preference for all these complexes.

In contrast, covalent bonds in transition metals comprise s and d orbitals. The sd^n hybrid orbitals may prefer bite angles that are either less than or greater than 90°, and it has been shown for highly covalent systems that the preferred bite angle depends on the number of d orbitals that are available to participate in the bonding.[53] This dependence is summarized in Table 5. The influence of such bite angle preferences explains most of the deviations from the main group behavior exhibited by the transition metals in Figure 14. The only transition metal that follows the main group trend, Cr^{III}, is predicted to have a 90° bite angle preference in common with the main group elements. The transition metals that show the largest deviations from the main group trend, Ti^{IV} and V^{IV}, are predicted to have the most acute bite angle preferences.

Although they are approximately the same size, differences in bonding result in a significantly reduced bite for Ti^{IV} when compared with that of Ga^{III}, and this structural change acts to lower the barrier heights for Ti^{IV} stereoinversion. When the normalized bites are computed from the M−O and O−O distances experimentally observed in the D_3 ground-state structures, the Kepert model correctly predicts the trend in barrier heights observed by experiment and predicted by DFT calculation. For example, normalized bites of 1.27 Å (Ti^{IV}), 1.31 (Ga^{III}), and 1.35 Å (Ge^{IV}) from the tris-catecholate complexes predict the observed trend $Ti^{IV} < Ga^{III} < Ge^{IV}$.[61] This result confirms that steric factors arising from repulsions in the inner coordination sphere play a key role in determining the relative barrier heights for this series.

As discussed above, the difference in bonding between main group and transition metal ions is expected to exert an additional influence on the rearrangement rates for Ti^{IV}. As anticipated, inspection of the calculated orbitals for the $[TiL_3]^{2-}$ transition-state structures reveals the participation of the Ti^{IV} d orbitals in both σ- and π-bonding interactions with the catecholate oxygens.

For the Bailar twist D_{3h} symmetric transition state of $[Ti(cat)_3]^{2-}$, graphic representations have been generated for those molecular orbitals including the highest percentages of d orbital involvement (Figure 15). Although the $[Ti(cat)_3]^{2-}$ complex is far from the covalent limit observed in the trigonal prismatic $[Zr(CH_3)_6]^{2-}$, the similar metal-centered directionality in Ti^{IV} acts to stabilize the trigonal prismatic geometry. Mulliken population analysis on the three geometries determined for $[Ti(cat)_3]^{2-}$ shows that there is significant electron density in the d orbitals, decreasing slightly on going from the ground state (2.26 e) to the trigonal prism (1.99 e) to the C_{2v} transition state (1.96 e).

Summary and Conclusion

The d^0 Ti^{IV} tris catecholate complexes undergo intramolecular isomerization faster than their d^{10} Ga^{III} and Ge^{IV} analogues. The solution behavior of Ti^{IV} tris catecholate complexes is qualitatively similar to that found for analogous Ga^{III} complexes. Based on the small and negative $\Delta S^{\ddagger}$ values for $[Ti\mathbf{2}_3]^{2-}$ racemization, the small differences in the activation parameters determined in different solvents, the strong parallels to the GaL_3 studies and the demonstrated stability of Ti^{IV} catecholate interactions, the contribution of bond-rupture isomerization mechanisms appears to be minimal. Both Bailar and Rây−Dutt mechanisms are operative, as evidenced by the solution behavior of $[Ti\mathbf{4}_3]^{2-}$, with the Bailar twist of *mer*-$[Ti\mathbf{4}_3]^{2-}$ faster than the Rây−Dutt isomerism of the *fac* and *mer* isomers. A Bailar process for *fac*-$[Ti\mathbf{4}_3]^{2-}$ could not be distinctly identified or characterized. Studies of the $[Ti\mathbf{1}_3]^{2-}$ and $[Ti\mathbf{3}_3]^{2-}$ complexes corroborate both the relationship between the Bailar and Rây−Dutt mechanisms, as well as that between the steric bulk of ligand substituents and the rate of complex isomerization.

The facile isomerization of the Ti^{IV} complexes is attributed to the availability of the empty d orbitals of Ti^{IV} for participation in metal−ligand bonds. This bonding results in a reduced ligand bite that decreases steric repulsion in the inner coordination sphere, stabilizing both possible transition states. In addition, covalent bonding to d^0 transition metals provides an additional stabilization to the D_{3h} and C_{2v} transition states that is not possible with main group metals. The results reflect the significance of d orbital involvement in transition metal bonding for d^0 metal ions and demonstrate the broader significance of these effects beyond $M(CH_3)_6$ structures.

Experimental Section

General. All reagents were obtained from commercial suppliers and used without further purification. Ligands $H_2\mathbf{1}$, $H_2\mathbf{2}$, $H_2\mathbf{3}$, and $H_2\mathbf{4}$ were synthesized according to previous reports.[5] ^1H and ^{13}C NMR spectra were recorded on Bruker 400 or 500 MHz instruments. Chemical shifts are reported as δ in ppm and referenced to residual solvent peaks. Mass spectra were recorded at the UCB Mass Spectrometry Facility, and elemental analyses were performed at the UCB Analytical Facilities.

Metal Complex Syntheses. $Na_2[Ti\mathbf{1}_3]$. To $H_2\mathbf{1}$ (67.1 mg, 0.344 mmol) and $TiO(acac)_2$ (29.8 mg, 0.114 mmol) was added 10 mL of degassed, anhydrous DMF. The solution turned dark red within minutes and was heated for 14 h at 150 °C under a nitrogen atmosphere. The solution was cooled to room temperature, and $NaHCO_3$ (23.7 mg, 0.282 mmol) was added as an aqueous solution (~2 mL), causing the reaction mixture to turn bright orange-red. The reaction mixture was evaporated to dryness, dissolved in methanol, and filtered through Celite. Removal of the methanol left a bright orange solid, which was washed with acetone and ether and dried under vacuum. Yield: 71.2 mg (81.1%). ^1H NMR (500 MHz, CD_3OD): δ 7.16 (dd, ^3J = 7.9 Hz, ^4J = 1.7 Hz, 3H, Ar*H*), 6.51 (t, J = 7.8 Hz, 3H, Ar*H*), 6.46 (dd, ^3J = 7.6 Hz, ^4J = 1.7 Hz, 3H, Ar*H*), 4.06 (m, J = 6.5, 3H, C*H*), 1.19 (d, J = 6.5 Hz, 3H, CH_3NH). $^{13}C\{^1H\}$ NMR (125 MHz, CD_3OD): δ 167.7, 163.4, 158.7, 117.5, 116.6, 114.5, 113.4, 41.0, 21.8. ES(−)-MS: m/z 628.1 $[M - 2Na + H]^-$, 313.7 $[M - 2Na]^{2-}$. Anal. Calcd (found) for $Na_2TiC_{30}H_{33}N_3O_9 \cdot {}^1/_2DMF \cdot 3{}^1/_2H_2O$: C 48.94 (48.84), H 5.67 (5.21), N 6.34 (6.56).

$K_2[Ti\mathbf{1}_3]$. Preparation of this complex from $H_2\mathbf{1}$ (46.2 mg, 0.237 mmol), $TiO(acac)_2$ (19.5 mg, 0.0743 mmol), and a 0.49 M methanolic KOH solution (480 μL, 0.24 mmol) was analogous to that described for $Na_2[Ti\mathbf{1}_3]$. Yield: 46 mg. Crystals suitable for X-ray diffraction grew at room temperature over several weeks from the diffusion of ethyl acetate into a DMF solution of the complex. ^1H NMR (500 MHz, CD_3OD): δ 7.16 (dd, ^3J = 7.9 Hz, ^4J = 1.5 Hz, 3H, Ar*H*), 6.50 (t, J = 7.7 Hz, 3H, Ar*H*), 6.46 (dd, ^3J = 7.6 Hz, ^4J = 1.5 Hz, 3H, Ar*H*), 4.05 (m, J = 6.3, 3H, C*H*), 1.18 (d, J = 6.5 Hz, 18H, CH_3).

$Na_2[Ti\mathbf{2}_3]$. The compound was prepared from $H_2\mathbf{2}$ (95.4 mg, 0.340 mmol), $TiO(acac)_2$ (29.5 mg, 0.113 mmol), and $NaHCO_3$ (19.4 mg, 0.231 mmol) following a procedure analogous to that described for $Na_2[Ti\mathbf{1}_3]$. Yield: 96.1 mg (88.5%). Crystals suitable for X-ray diffraction grew at room temperature from the diffusion of ethyl acetate into a DMF solution of the complex. ^1H NMR (400 MHz, CD_3OD): δ 7.24 (s, 6H, Ar*H*), 4.08 (sept, J = 6.5 Hz, 6H, C*H*CH_3), 1.20 (br s, 36 H, CH_3). $^{13}C\{^1H\}$ NMR (100 MHz, CD_3OD): δ 168.2, 161.2, 118.2, 117.8, 42.7, 23.6. ES(−)-MS: m/z 905.4 $[M - Na]^-$, 883.4 $[M - 2Na + H]^-$, 441.3 $[M - 2Na]^{2-}$. Anal. Calcd (found) for $Na_2TiC_{42}H_{54}N_6O_{12} \cdot 2H_2O$: C 52.29 (52.18), H 6.06 (6.17), N 8.71 (8.67).

$K_2[Ti\mathbf{2}_3]$. The compound was prepared from $H_2\mathbf{2}$ (73.5 mg, 0.262 mmol), $Ti(O^iPr)_4$ (22 μL, 0.074 mmol), and $KHCO_3$ (15.1 mg, 0.151 mmol) following a procedure analogous to that described for $Na_2[Ti\mathbf{1}_3]$. Yield: 60 mg (79%). ^1H NMR (400 MHz, CD_3OD): δ 7.24 (s, 6H, Ar*H*), 4.09 (m, J = 6.5 Hz, 6H, C*H*), 1.20 (br s, 36H, CH_3). $^{13}C\{^1H\}$ NMR (100 MHz, CD_3OD): δ 168.2, 161.2, 118.2, 117.8, 42.7, 23.6. Anal. Calcd (found) for $K_2TiC_{42}H_{54}N_6O_{12} \cdot 3{}^1/_2H_2O$: C 49.26 (49.22), H 6.00 (6.06), N 8.21 (8.03).

$Na_2[Ti\mathbf{3}_3]$. The compound was prepared from $H_2\mathbf{3}$ (65.6 mg, 0.390 mmol), $TiO(acac)_2$ (33.7 mg, 0.129 mmol), and $NaHCO_3$ (26.5 mg, 0.316 mmol) following a procedure analogous to that described for $Na_2[Ti\mathbf{1}_3]$. Yield: 71.1 mg. ^1H NMR (500 MHz, CD_3OD): 7.20 (d, ^3J = 7.9 Hz, ^4J = 1.6 Hz, 3H, Ar*H*), 6.53 (t, J = 7.8 Hz, 3H, Ar*H*), 6.49 (d, ^3J = 7.6 Hz, ^4J = 1.6 Hz, 3H, Ar*H*), 2.91 (s, 9H, CH_3). $^{13}C\{^1H\}$ NMR (125 MHz, CD_3OD): δ 170.8, 160.8, 160.4, 119.4, 118.5, 116.4, 115.3, 26.3. ES(−)-MS: m/z 566.1 $[M - Na]^-$, 544.1 $[M - 2Na + H]^-$, 271.7 $[M - 2Na]^{2-}$.

$K_2[Ti\mathbf{4}_3]$. The compound was prepared from $H_2\mathbf{4}$ (51.2 mg, 0.150 mmol), $TiO(acac)_2$ (12.4 mg, 0.0473 mmol), and $KHCO_3$ (13.4 mg, 0.134 mmol) in 10 mL of degassed, anhydrous DMF following a procedure analogous to that described for $Na_2[Ti\mathbf{1}_3]$. Yield: 46.9 mg (78%). ^1H NMR (500 MHz, CD_3OD): (see Figure 13, spectrum is broad at room temperature). $^{13}C\{^1H\}$ NMR (125 MHz, CD_3OD): δ 169.1, 169.0, 167.9, 160.9, 139.9, 129.8, 128.1, 128.0, 118.3, 118.1, 117.7, 117.6, 68.3, 44.1, 29.4, 24.0. +FAB-MS (TGG) (Na_2 salt): m/z 1137 $[M + Na]^+$, 1115 $[M + H]^+$, 1093 $[M + 2H - Na]^+$. Anal. Calcd (found) for $K_2TiC_{57}H_{60}N_6O_{12} \cdot 7H_2O$: C 53.77 (53.97), H 5.86 (5.33), N 6.60 (6.56).

$K_2[Ge\mathbf{2}_3]$. To $H_2\mathbf{2}$ (158 mg, 0.563 mmol) dissolved in anhydrous DMF (5 mL) was added $Ge(O^iPr)_4$ (48.0 μL, 0.161 mmol) via microsyringe. The reaction solution was heated under a nitrogen atmosphere at 120 °C. After 72 h the reaction was cooled to room temperature, and $KHCO_3$ (34.5 mg, 0.341 mmol) was added as a solution in 0.5 mL of water. The solvent was removed by rotary evaporation. The germanium complex was purified by elution with methanol on a sephadex LH-20 column. Yield: 138 mg (83%). Crystals suitable for X-ray diffraction grew at room temperature over several weeks from the diffusion of acetone into an ethanol solution of the

complex. ^{1}H NMR (400 MHz, CD_3OD): δ 9.27 (d, J = 6.2 Hz, 6H, N*H*), 7.17 (s, 6H, Ar*H*); 4.03 (m, J = 6.6 Hz, 6H, C*H*); 1.21 (d, J = 6.5 Hz, 18H, CH_3), 1.03 (d, J = 6.5 Hz, 18H, CH_3). ^{13}C NMR (100 MHz, CD_3OD): δ 166.78, 150.91, 116.39, 115.31, 40.94, 22.06, 21.48. ES(−)-MS: *m*/*z* 947.3 [M − K]$^-$, 931.3 [M − 2K + Na]$^-$, 909.3 [M − 2K + H]$^-$. Anal. Calcd (found) for $K_2GeC_{42}H_{54}N_6O_{12}\cdot 3H_2O$: C, 48.52 (48.52); H, 5.82 (5.70), N 8.08 (7.81).

K_2[Ge4$_3$]. To H_2**4** (60.7 mg, 0.177 mmol) dissolved in anhydrous DMF (5 mL) was added Ge(O^{i}Pr)$_4$ (15.0 μL, 0.050 mmol) via microsyringe. The reaction solution was heated under a nitrogen atmosphere at 120 °C. After 72 h the reaction was cooled to room temperature, and $KHCO_3$ (11.0 mg, 0.109 mmol) was added as a solution in 0.5 mL of water. The solvent was removed by rotary evaporation. The germanium complex was purified by elution with methanol on a sephadex LH-20 column. Yield: 38.3 mg (61%). ^{1}H NMR (400 MHz, CD_3OD): δ. 9.70 (m, N*H*), 9.32 (m, N*H*), 8.00 (s, Ar*H*), 7.28−7.04 (m, Ar*H*), 4.56−4.28 (m, CH_2) 1.32 (s, CH_3), 1.26 (s, CH_3), 1.25 (s, CH_3), 1.17 (s, CH_3). ^{13}C NMR (100 MHz, CD_3OD): δ. ES(−)-MS: *m*/*z* 1133.4 [M − K]$^-$, [M − 2K + Na]$^-$, 1095.4 [M − 2K + H]$^-$. Anal. Calcd (found) for $K_2GeC_{57}H_{60}N_6O_{12}\cdot 4H_2O$: C, 55.03 (54.97); H, 5.51 (5.31), N 6.76 (6.64).

X-ray Crystallographic Studies. Suitable crystals of each compound were mounted on glass capillaries using Paratone-N hydrocarbon oil and cooled by a nitrogen flow low-temperature apparatus during data aquisition. Crystal data for K_2[Ti**1**$_3$]·3DMF, Na_2[Ti**2**$_3$]·5DMF, and K_2[Ge**2**$_3$]·4C_3H_6O were collected on a Bruker SMART[63] diffractometer, equipped with a CCD area detector using Mo Kα (λ = 0.71073) radiation. Data in the frames corresponding to an arbitrary hemisphere of data were integrated using SAINT.[64] The data were corrected for Lorentz and polarization effects. An empirical absorption correction based on the measurement of redundant and equivalent reflections and an ellipsoidal model for the absorption surface were applied with the use of SADABS.[65] The structure solution and refinement for all structures were performed using SHELXTL (refining on F^2).[66] Hydrogen atoms were included but not refined. Further crystallographic information can be found in the captions to Figures 4 and 9 and in the Supporting Information.

Variable-Temperature ^{1}H NMR Measurements. Variable-temperature measurements were carried out on a Bruker DRX 500 spectrometer operating at 500 MHz. The temperature was controlled by the BVT-3000 temperature unit, which ensures a precision of ±0.1 °C. The probe temperature was allowed to equilibrate for 15 min prior to final magnetic homogeneity optimization on the lock signal. Each temperature point was calibrated with a methanol or ethylene glycol standard. Each sample was prepared as a 20 mM solution in CD_3OD. Line shape analysis of experimental spectra was executed using the Mexico fitting software.[38]

DFT Calculations. Calculations were performed using the NWChem program.[67] Ground-state and transition-state geometries for all complexes were optimized using the hybrid B3LYP functional[68] and all-electron polarized double-ζ basis sets.[69] The DZVP2 basis set was used for all atoms with the exception of Ge and Ga, for which the DZVP basis set was used. Initial geometries were placed in either D_3, D_{3h}, or C_{2v} symmetry, and the optimizations were constrained to maintain the starting symmetry. Frequency calculations, performed on the smaller tris-catecholate structures, verified that the optimized geometries were either minima (no negative frequencies) or maxima (one negative frequency) on the potential energy surface. ECCE software was used to render molecular orbital images.[70]

Acknowledgment. We thank Drs. A. Oliver and F. Hollander for structure determination assistance and Dr. J. Xu for experimental support. A.V.D and K.N.R. were funded by NSF grant CHE-9709621. B.P.H. and T.K.F. acknowledge support from the Environmental Management Science Program (Grant 73759), Office of Science, U.S. Department of Energy (DOE). DFT calculations were performed using the Molecular Science Computing Facility in the William R. Wiley Environmental Molecular Sciences Laboratory located at the Pacific Northwest National Laboratory (operated for DOE by Battelle) and funded by the DOE's office of Biological and Environmental Research.

Supporting Information Available: Experimental and simulated VT ^{1}H NMR spectra for K_2[Ti**2**$_3$] in DMF-d_7 and D_2O; VT ^{1}H NMR of [Ti**2**$_3$]$^{2-}$ as a function of counter ion (Na^+, K^+), concentration, and added base; VT ^{1}H NMR of K_2[Ge**2**$_3$] in D_2O (pD 8.6); Eyring plots; X-ray structure information for K_2[Ti**1**$_3$]·3DMF, Na_2[Ti**2**$_3$]·5DMF, and K_2[Ge**2**$_3$]·4C_3H_6O; DFT results for D_3 ground-state and D_{3h} and C_{2v} transition-state calculations for [Ti(cat)$_3$]$^{2-}$, [Ti**B**$_3$]$^{2-}$, [Ga(cat)$_3$]$^{3-}$, [Ga**B**$_3$]$^{3-}$, [Ge(cat)$_3$]$^{2-}$, and [Ge**B**$_3$]$^{2-}$; complete refs 67 and 70. This material is available free of charge via the Internet at http://pubs.acs.org.

JA0617946

(63) *SMART, Area Detector Software Package*; Siemens Industrial Automation, Inc.: Madison, 1995.
(64) *SAINT, SAX Area Detector Integration Program*, V4.024; Siemens Industrial Automation, Inc.: Madison, 1995.
(65) Sheldrick, G. *SADABS, Siemens Area Detector Absorption Correction Program*; advance copy, 1996.
(66) Sheldrick, G. *Crystal Structure Determination Software Package*; Siemans Industrial Automation, Inc.: Madison, WI, 1993.
(67) Straatsma, T. P.; et al. *NWChem, A Computational Chemistry Package for Parallel Computers*, 4.6; Pacific Northwest National Laboratory: Richland, Washington, 2004.
(68) Becke, A. D. *Phys. Rev. A* **1988**, *38*, 3098−3100.
(69) Godbout, N.; Salahub, D. R.; Andzelm, J.; Wimmer, E. *Can. J. Chem.* **1992**, *70*, 560−571.
(70) Black, G.; et al. *Ecce, A Problem Solving Environment for Computational Chemistry, Software*, 3.2.2; Pacific Northwest National Laboratory: Richland, Washington, 2005.